Article:
Litvinov, V, Deblieck, R, Clair, C et al. (6 more authors) (2020) Molecular Structure, Phase Composition, Melting Behavior, and Chain Entanglements in the Amorphous Phase of High-Density Polyethylenes. Macromolecules, 53 (13). pp. 5418-5433. ISSN 0024-9297

https://doi.org/10.1021/acs.macromol.0c00956

Molecular Structure, Phase Composition, Melting Behavior and Chain Entanglements in the Amorphous Phase of High-Density Polyethylenes

Victor Litvinov,*[,1] Rudy Deblieck,[2,3] Charles Clair,[4] Winke Van den fonteyne,[2] Abdelaziz Lallam,[4] Ralf Kleppinger,[2,3] Dimitri A. Ivanov,[5,6,7,8] Michael E. Ries,[9] and Mark Boerakker[2]

[1] V.Lit.Consult, Gozewijnstraat 4, 6191WV, Beek, The Netherlands

[2] SABIC, Technology and Innovation, Geleen, The Netherlands

[3] DSM Materials Science, Geleen, The Netherlands

[4] Laboratoire de Physique et Mécanique Textiles, F-68093 Mulhouse Cedex, France

[5] Institut de Sciences des Matériaux de Mulhouse-IS2M, CNRS UMR 7361, F-68057 Mulhouse, France

[6] Lomonosov Moscow State University, Faculty of Fundamental Physical and Chemical Engineering, Leninskie Gory 1/51, 119991 Moscow, Russian Federation

[7] Moscow Institute of Physics and Technology (State University), Institutskiy per. 9, Dolgoprudny, 141700, Russian Federation

[8] Institute of Problems of Chemical Physics, Russian Academy of Sciences, Chernogolovka, Moscow region, 142432, Russian Federation

[9] School of Physics & Astronomy, University of Leeds, Leeds, LS2 9JT, UK

ABSTRACT: A methodology for estimating the entanglement density in the amorphous phase of semicrystalline polyolefins was developed. The method is based on the analysis of the density of physical network junctions in the amorphous phase by ^{1}H NMR T_2 relaxation experiments in the

melting temperature range. Melting-induced changes in phase composition and chain motion in crystalline and amorphous phases were studied for melt- and high-pressure crystallized high-density polyethylenes (HDPE). The density of the entanglement network was estimated at temperatures close to and gradually approaching melting. Its value is lower for high-pressure crystallized HDPE than for the same melt-crystallized polymer. The network of entanglements is characterized by the fraction of entangled network chains, the weight average molecular weight of the network chains between apparent chain entanglements, M_e, and the volume average density of apparent chain entanglements. The entanglement network was studied in a series of low and high molecular weight HDPE, and bimodal HDPE samples with different molecular weight characteristics and densities controlled by different content of butene comonomer. It turns out that the molecular weight characteristics of the HDPE's influence the entanglement network. The fraction of network chains and average density of apparent chain entanglements decrease with decreasing molecular weight M_n due to the "diluting" effect caused by disentangled chain-end segments increasing the value of M_e. The current methodology is of interest for studying the effect of crystallization conditions, molecular structure and short-chain branches on phase composition, melting behavior and chain entanglements in the amorphous phase of polyolefins. The method allows estimation of the fraction of entangled network chains which potentially can form tie chain segments during deformation. The effect of short chain branches and molecular weight characteristics on the creep response of polyolefins is discussed.

For Table of Content use only

Molecular Structure, Phase Composition, Melting Behavior and Chain Entanglements in Amorphous Phase of High-Density Polyethylenes

Victor Litvinov, Rudy Deblieck, Charles Clair, Winke Van den fonteyne, Abdelaziz Lallam, Ralf Kleppinger, Dimitri A. Ivanov, Michael E. Ries and Mark Boerakker

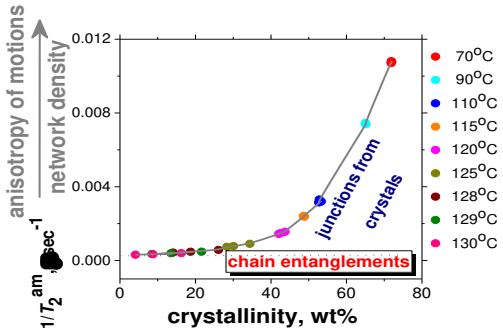

1. INTRODUCTION

The physical and mechanical properties of polymers are a complex interplay of molecular structure, processing conditions and resulting morphology.[1] Variation of molecular structure elements, i.e., the molecular weight distribution, type and number of comonomer units, length of long-chain branches and their distribution are explored for production of a wide range of polyolefins and their blends with largely different properties.[2,3,4,5,6,7,8,9,10,11,12,13,14,15,16]

By now it is widely accepted that the "amorphous phase of the bulk polymer plays a pre-dominant role in many aspects of the properties of semicrystalline polymers".[17] The dynamic network of remnant chain entanglements in the amorphous phase of a semicrystalline polymer affects the toughness, the strength of the interfacial adhesion in polymer composites, the strain hardening modulus, the resistance to creep failure, craze crack failure and the rate of the slow crack growth by craze propagation.[18,19,20,21,22] The ductile failure regime of high density polyethylene (HDPE) pipes shows a time resilience that depends on the crystallization history and on the chemical structure. It is now assumed that this is caused by a change of the network density due to disentangling by crystallization, leading to a lower initial average density of the entanglement network as compared to the network density in the melt. If this is so, the melt elasticity coming from the solid state should show a relaxation when it reverts to the melt state equilibrium value.[23]

Chain entangling is an intrinsic property of long-chain molecules which originates from the uncrossability of neighboring chains surrounding a given chain. There are two complementary physical views on chain entanglements in polymer melts: (1) a continuous tube confining transverse motions of a given chain; and (2) discrete binary entanglement nodes with neighboring chains, i.e., the topological entanglement concept.[24,25,26] Entanglement density in semicrystalline polymers can be affected by crystallization conditions from the melt,[23,27] polymer concentration for solution-crystallized polymers,[28,29] and for nascent powders - by the type of catalyst used and

polymerization conditions.[30] Crystallization of polymers from the molten state under shear flow can also affect the entanglement density in the amorphous phase.[31] Estimation of the entanglement density in a semicrystalline state is still an unresolved issue. Several solid-state NMR studies provided indirect information on difference in the entanglement density in PE's at temperatures below melting.[32,33,34] The difference in the entanglement density is reflected in the phase composition, chain motion in PE crystals (α-crystalline relaxation process), long-range chain diffusion between crystalline and amorphous domains, and the type of crystal-amorphous interface.[33] Many other structures of semicrystalline polymers such as lamellae thickness, morphology, chain-folding structure as well as crystallization kinetics are also affected by entanglements of polymer chains.[27,35,36]

Proton NMR T_2 relaxation experiments are very sensitive to even small changes in the density of chemical and physical network junctions.[37,38] The network junctions increase the anisotropy of segmental motion, which causes an increase in the strength of interactions between nuclear spins resulting in a more efficient T_2 relaxation. These inter-nuclear interactions are quantified by different NMR experiments and the obtained values are used for calculating the molecular weight of network chains.[37,38,39] However, this method was not explored for estimating entanglement density in the amorphous phase of semicrystalline polymers.

At temperatures well above T_g, the NMR T_2 relaxation time of the amorphous phase is determined not only by chain entanglements but also by junctions which originate from polymer crystals providing a dense network in the amorphous phase. Moreover, polymer crystals impose constraints on translational chain motions in the amorphous phase. The constraints also increase the anisotropy of the segmental motion and thereby cause an additional decrease in the T_2 relaxation time. In order to separate the effect of chain entanglements from restrictions on segmental motion from polymer crystals, the T_2 relaxation analysis should be performed in a temperature range which

is close to the end of melting. In this case of vanishing crystalline restrictions, chain entanglements provide the major contribution to the T_2 relaxation time of the amorphous phase.

The driving force and aim of this study is to find out whether the solid-state ^{1}H NMR T_2 relaxometry can be used to assess the density of the remnant chain entanglements in semi-crystalline polyethylenes. This remnant network of entanglements is formed by the entanglements which are left over after partial disentangling, if this occurs, during crystallization. It is also a source of potential tie molecules. The larger the number of tie molecules, which are effective on the time scale of the load, the slower the crack growth will be.[18,22] The presence of such a remnant network can be probed *indirectly* via mechanical observables such as creep rate deceleration (CRDF),[11] strain hardening,[40] natural draw ratio,[41] and the rubber plateau in solid and melt states.[23] Therefore, there is a need for a *direct* method to estimate the entanglement density in the amorphous phase of polyolefins.

A series of melt-crystallized high-density bimodal HDPEs with different butene comonomer content and molecular weight, high- and low- (M_n = 3.6 kg/mol) molecular weight HDPE, nascent ultra-high molecular weight HDPE powder (UHMWPE), and high-pressure crystallized HDPE are studied in the present work. The T_2 relaxation experiments, which should be performed in the melting temperature range, require special attention because fast partial melting and re-crystallization processes can occur. The rate of sample heating and the time needed for temperature stabilization within the sample volume were determined by a real-time T_1 relaxation experiment.[42] Because the NMR T_2 relaxation experiment near the melting temperature should be performed as fast as possible, the measuring time was reduced to less than two minutes by optimizing sampling of data points and data acquisition. The effect of chain entanglements and short chain branches on CRDF of the bimodal HDPE's is discussed in the last section of the paper.

2. EXPERIMENTAL SECTION

2.1. Characterization of HDPE Samples. HDPE samples with different molecular weight characteristics and amount of ethylene branches were studied (Table 1). All polymerization experiments were performed in a 20-liter bench-scale reactor, which was typically used with 10 liters of diluent and a Ziegler-Natta catalyst. The reactor pressure was controlled by the ethylene feed. The installation was equipped with an on-line gas chromatograph to monitor and control the concentrations and ratios of the hydrogen and 1-butene in the headspace. Two samples were synthesized with a single site FI catalyst, i.e., nascent UHMWPE powder (nUHss) and HDPE which was used for preparing high-pressure crystallized HDPE (hpc-HDPE). End groups and branch content were determined by solution-state ^{1}H NMR spectroscopy. Samples were dissolved at 130 °C in *tri*-chloroethylene stabilized by di-*tert*-butyl-*para*-cresol. ^{1}H NMR spectra were recorded at 120 °C on a 600 MHz NMR spectrometer. To determine the molecular weight distribution, high temperature size exclusion chromatography was applied. Samples were dissolved in *tri*-chlorobenzene. A Polymer Laboratories column (13 m PLgel Olexis, 300 x 7.5 mm) was used for the separation and detection with a Polymer Char IR5 detector. The calibration was performed using linear polyethylene standards.

Table 1. Molecular Weight and Molecular Weight Distributions of HDPE Samples. *

Sample	Ethyl branches per 1000C	M_n, kg/mol	M_w, kg/mol	M_z, kg/mol	PDI	Butene, wt.%
biHMHB	6.4	7.8	330	2200	42.3	2.6
biHMLB	2.4	8.6	335	2000	39.0	1.0
biLMHB	8.3	7.9	175	1000	22.2	3.3

biLMLB	3.9	7.7	195	1200	25.3	1.6
R2HMHB	11.5	89	610	2000	6.85	4.6
R2HMLB	5.0	110	720	2400	6.55	2.0
R2LMHB	14.3	57	340	1200	5.96	5.7
R2LMLB	7.7	61	330	960	5.41	3.1
R1	0.2	3.6	33	440	9.17	0.08
nUHss	-	660	1600	4000	2.42	-
mc-HDPE	-	95	260	-	2.74	-
hpc-HDPE	-	95	260	-	2.74	-

* The samples designation is given according to the molecular weight characteristics and the number of branches: bi – bimodal, HM and LM – high and low molar mass, HB and LB – high and low branch content. R1 and R2 corresponds to HDPE synthesized in reactors 1 and 2. nUHss is nascent UHMWPE powder, mc-HDPE and hpc-HDPE correspond to melt- and high-pressure crystallized HDPE, respectively.

The following time-temperature-pressure profile was used for preparing compression-molded sheets of bimodal, R1 and R2 HDPE's. The samples were kept in the mold for 300 sec at 180 °C and a pressure of 0.39 MPa, then pressure was increased to 4.71 MPa. After 180 sec, the pressure was decreased to 0.08 MPa and samples were kept in the mold for 900 sec. After that, the samples were cooled in the mold with at a rate of 1.7 °C/sec. The mold was opened when its temperature reached 25 °C. The thickness of these compression-molded sheets was approximately 0.35 mm.

High-pressure crystallized HDPE (hpc-HDPE) was prepared using the following procedure. A cylindrical high-pressure cell for isothermal and isobaric crystallization was used. The cell had a diameter of 6 mm. The sample was melted in the cell at 235 °C under atmospheric pressure. Then,

a pressure of 630 MPa was applied for 1 hour using a Zwick Roell materials testing machine (Zwick Z010) which was set to a creep test mode. This allowed determining the completion of crystallization by measuring the volume decrease due to crystallization. After crystallization was completed, the sample was cooled down to 60 °C under pressure and then the pressure was released.

The melting behavior of all samples was determined using first heating of samples at a heating rate of 10 °C/min (Table 2). Annealing experiments at different times and temperatures were performed using a Perkin Elmer DSC. Samples were heated from -40 °C to annealing temperature at a heating rate of 10 °C/min. Annealing time in subsequent experiments was the following: 2, 4, 6, 10, 14, 18, 22, 26, 28 and 30 min. After each annealing time, sample was cooled to -40 °C with the rate of 10 °C/min and DSC traces was recorded again at heating rate of 10 °C/min. New samples were used for the experiment at each annealing time.

Table 2. Thermal Characteristics of HDPE Samples at First Heating.

Sample	Heat of fusion, *J/g*	Peak melting temperature, °C
biHMHB	172	128.6
biHMLB	201	130.1
biLMHB	179	127.9
biLMLB	189	129.2
R2HMHB	105	121.0
R2HMLB	137	126.7
R2LMHB	107	120.5
R2LMLB	133	123.7
R1	243	132.4

nUHss	220	145.2
mc-HDPE	203	136.1
hpc-HDPE	287	150.5

2.2. Tensile Creep Tests. Tensile creep tests were performed at 80 °C on an Instron tensile machine model 5564 using Bluehill software to program the test and output of the data. The sample was drawn at a true strain rate of 1.667 ± 0.001 10^{-3}/s until a set load. Details of the creep experiment and data analysis are provided in Supporting Information S1.1. The accuracy of the creep rate deceleration factor was ± 3%.

2.3. X-Ray Synchrotron Studies. Simultaneous small- and wide-angle X-ray scattering (SAXS/WAXS) experiments were carried out at the ID02 beamline of the ESRF (Grenoble, France). The measurements were conducted in transmission geometry using a photon energy of 12.46 keV, the corresponding wavelength being 0.995 Å. The monochromatic incident X-ray beam was collimated to a footprint of 100 x 200 μm² (V x H) on the sample. The estimated total photon flux on the sample was 9.10^{11} photons per second which enabled acquisition times of less than 100 ms per frame. The accessed s values, with $s = 2sin(\Theta)/\lambda$ where Θ is the Bragg angle and λ – the wavelength, covered a range from $4.8 \cdot 10^{-3}$ nm^{-1} to $4.8 \cdot 10^{-1}$ nm^{-1} using a sample-to-detector distance of 2.5 m. A Rayonix MX-170HS detector implemented in a 35 m long vacuum flight tube was applied for the recording of the SAXS intensity, while a Rayonix LX-170HS detector was used for the WAXS experiments. More details on the data treatment including computation of the 1D interface distribution function can be found in section 4 of the Supporting Information.

2.4. Time-Domain ^{1}H NMR Experiments. Proton NMR transverse magnetization relaxation (T_2 relaxation) experiments were performed for static samples on a Bruker Minispec MQ-20

relaxometer equipped with 10 mm temperature probe head. The relaxometer operates at a proton resonance frequency of 19.65 MHz. The length of the 90° pulse, the dead time of the probe head receiver and the dwell time were 2.8 μs, 7 μs and 0.5 μs, respectively. The temperature was pre-set by placing a 9 mm in diameter NMR tube with a Pt100 thermometer in the NMR probe head. The head of the thermometer was submerged in silicon oil at the tube bottom. Temperature was regulated with an accuracy higher than ± 0.5 °C using a Bruker BVT-3000 temperature controller.

The following experiments were used to record the decay of the transverse magnetization relaxation (T_2 decay) from chain segments with largely different mobility.

(1) The free induction decay (FID) of low mobile chain segments was recorded using single-pulse excitation (SPE): $90°_x$ – dead time – [acquisition of FID]. The amplitude of the FID for times t longer than approximately 150 - 200 μs was affected by the inhomogeneity of the magnetic field, which is due to the inhomogeneity of the permanent magnetic field B_o of the spectrometer (T_2^* of water was ≈ 1.1 ms) and the B_o inhomogeneity within a sample volume that arises from an inhomogeneous magnetic susceptibility of heterogeneous samples.

(2) Hahn-echo pulse sequence (HEPS) was used for recording the T_2 decay of the mobile chain segments: $90°_x$ - t_{He} - $180°_y$ - t_{He} - [acquisition of the amplitude of an echo maximum $A(t)$ as a function of echo time - $2 \cdot t_{He}$]. Value of t_{He} was varied from 35 μs to 100 msec. The HEPS was used to record the slow part of the T_2 relaxation decay, which is caused by the relaxation of mobile chain segments. The amplitude of the transverse magnetization relaxation, which was determined by the SPE and the HEPS experiments for semicrystalline HDPE, was the same in the time interval from about 120 μs to 150 μs. Therefore, the results of the both experiments were combined in this time interval in a single file (Figure 1). The combined file was used for determining the phase

composition and chain motions in HDPE samples below the melting temperature range. T_2 decay of molten samples was recorded with the HEPS as described previously.[38]

(3) The T_2 relaxation decay in the *melting temperature range* was recorded using SPE and HEPS methods, which were combined in one experiment (SPE+HEPS): $90°_x$ – dead time – [acquisition of the free induction decay (FID)] - t_{He} - $180°_y$ - t_{He} - [acquisition of the amplitude of an echo maximum $A(t)$ as a function of echo time].

(4) The ^{1}H spin-lattice relaxation time T_1 was measured using a saturation-recovery pulse sequence consisting of 90° saturation pulses followed by a solid-echo pulse sequence: $[(90°_x - \tau)_n - t_{sat} – (90°_x - \tau_{se} - 90°_y) –$ (acquisition of solid-echo decay) - repeated experiment with new value of t_{sat}]. t_{sat} is recovery time after the saturation pulses $(90°_x - \tau)_n$, τ and τ_{se} were 1 ms and 10 μs, respectively, and $n = 20$.

The recycle delay time for the all T_2 experiments was longer than five times T_1. A more detailed discussion of the NMR experiments is provided in the Supporting Information S1.2.

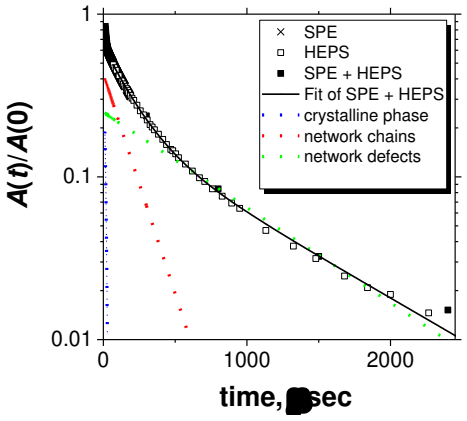

Figure 1. ^{1}H NMR T_2 relaxation decay for HDPE sample R2HMHB. The decay was measured at 100 °C using SPE, HEPS and SPE+HEPS experiments. The solid line represents the result of a least-square adjustment of the combined SPE + HEPS decays (points) with a linear combination of a Gaussian and two

exponential functions. The dotted lines show the separate relaxation components that originate from the relaxation of the crystalline phase, the network chains and the network defects as it will be shown below.

2.5. Heating Rate of Samples in the Probe head of the NMR Relaxometer. The rate of sample heating should be known for performing experiments in the melting temperature range. For this purpose, the T_1 NMR relaxation experiment was used (Supporting Information S1.3).[42] Five minutes were needed for the temperature stabilization within the sample volume after the NMR tube with the sample was placed in the NMR probe head heated to the required temperature. This time was taken as zero in all real-time NMR T_2 relaxation experiments.

2.6. Characterization of Phase Composition and Chain Motions by ^{1}H NMR T_2 Relaxometry. Proton NMR is a sensitive and robust method for determining phase composition and chain motions in complex multiphase polymers in cases of distinct chain motions in different phases.[43,44,45,46,47] The overall observed T_2 decay is a sum of contributions from all the phases. A suitable fitting routine is employed to deconvolute the contribution of the different phases to the T_2 decay in terms of relative concentrations and decay rates. Besides predicting the number of phases/components, the method is inherently quantitative in nature since the amplitude of the relaxation component for each phase is directly proportional to the number of protons present in that phase. FID for a few HDPE samples are compared in Supporting Information S1.2 (Figures S3 and S4). The strong dipolar couplings in the crystalline domains lead to an Abragamian shape of the FID for the crystalline phase.[48] A linear combination of an Abragamian, a Gaussian and two exponential functions provided the best description of the T_2 decay at 70 °C for R2 and bimodal HDPE's (Figure 1):

$$A(t) = A(0)^{cr} \exp[-(t/2T_2^{cr})^2] \cdot \left[\sin(\alpha t)/\alpha t\right] + A(0)^{in} \exp[-(t/T_2^{in})^2] + A(0)^{am} \exp[-(t/T_2^{am})]$$

$$+ A(0)^{r} \exp[-(t/T_2^{r})] \qquad (1)$$

A value of $\alpha = 0.166$ was used to fit the T_2 decay at 70 °C for the bimodal HDPE's and the R2 samples. The four relaxation components were assigned to the crystalline phase - (T_2^{cr} relaxation time); crystal-amorphous interface - (T_2^{in} relaxation time); soft amorphous fraction - (T_2^{am} relaxation time); and chain segments with high chain mobility which is typical for rubbers - (T_2^{r} relaxation time).[37,42] Since most CH_3 groups at the end of polymer chains reside in a nearly solid-like environment,[49] highly mobile chain segments mainly originate from short chain branches with adjacent ethylene units.[50] $A(0)^{index}$ is the amplitude of the relaxation components.

The transverse magnetization relaxation time T_2^{index} characterizes chain motions. The longer the T_2^{index}, the larger the frequency and/or the amplitude of chain motions are. It should be noted that the time constant of these functions (T_2 value) cannot be used for comparing the relative difference in chain mobility in different phases due to the difference in the shape factor of these relaxation components (Abragamian, Gaussian and exponential), and the difference in the origin of the NMR relaxation process in different phases. The relative fraction of the relaxation components, $\{A(0)^{index}/[A(0)^{cr} + A(0)^{in} + A(0)^{am} + A(0)^{r}]\}$ x 100%, represents the relative amount of hydrogen atoms (as expressed in weight fractions) of crystalline phase, of crystal-amorphous interface, and of chain segments with largely different anisotropy of chain motions in the amorphous domains. In general, crystallinity determination using different methods does not always yield the same results even when used on exactly the same sample due to reasons discussed previously.[44,45,46,51]

The phase composition of HDPE samples and T_2 relaxation time for each phase, which were determined at 70 °C, are shown in Supporting Information S1.4, Table S1. The effect of the molecular structure of HDPE on these physical structure characteristics is discussed in S1.4.

The rather fast chain diffusion in the crystalline phase in the melting temperature range - the α-relaxation process - causes a change in the shape of the T_2 decay of HDPE crystals from the Abragamian to the Gaussian one (α in equation 1 decreases with temperature increase). In the melting temperature range, the small amount of crystal-amorphous interface cannot be determined with sufficiently high accuracy due to the low crystallinity. Therefore, a three relaxation components model was used to describe the phase composition in this case. The T_2 decay can be well fitted using a linear combination of a Gaussian and two exponential functions:

$$A(t) = A(0)^{cr} \exp[-(t/T_2^{cr})^2] + A(0)^{net} \exp[-(t/T_2^{net})] + A(0)^{def} \exp[-(t/T_2^{def})] \quad (2)$$

The relaxation components were assigned to the crystalline phase - (T_2^{cr} relaxation time); the network chains, which are formed in the amorphous phase by chain entanglements and linkages of chain segments to PE crystals - (T_2^{net} relaxation time); and the highly mobile chain segments (network defects) in the amorphous phase - (T_2^{def} relaxation time) as it will be shown below.

2.7. Optimization of T_2 Relaxation Experiments for Fast Recording of the T_2 Decay in the Melting Temperature Range. In order to reduce the effect of structural reorganizations in the melting temperature range, the T_2 decay should be recorded with sufficiently high accuracy within a short time using SPE and HEPS experiments. An optimal sampling pattern was used to reduce the time required for recording the T_2 decay with the HEPS experiment.[52,53,54] Despite the smaller number of acquisitions and Hahn-echo times, the relaxation parameters, which were recorded using

the fast SPE+HEPS experiment, coincide within 5 % with those from separate SPE and HEPS experiments with larger number of data acquisitions and of HEPS data points (Supporting Information S1.5, Table S2).

2.8. Analysis of the Structure of Polymer Networks by NMR T_2 Relaxometry. NMR relaxometry is a well-established methodology that provides quantitative information on the density of network junctions, network heterogeneity and network defects.[55] The presence of network junctions, i.e., chemical cross-links and/or physical junctions, increases the anisotropy of chain motions which causes an increase in the strength of interactions between nuclear spins. The strength of the inter-nuclear interactions is quantified by different NMR experiments and its value is used for calculating molecular weight of network chains.[37,38,39,55,56,57] The distinguishing feature of the T_2 relaxation for polymer networks without defects is the plateau observed at temperatures well above the dynamic glass transition temperature T_g^d.[56,57,58] T_g^d of the NMR method is observed at temperature 20 – 30 °C higher than T_g determined by low-frequency methods such as DSC and low-frequency dynamic mechanical thermal analysis. The difference in the temperatures is expected from the time-temperature-superposition-principle.[59] The temperature-independence of T_2 for the network chains at the plateau (T_2^{pl}) is attributed to constraints, which limit the number of possible conformations of a network chain relative to those of a free chain. Suggesting the Gaussian chain statistics and fixed position of network junctions, the theory of transverse relaxation of polymer networks relates T_2^{pl} to the number of statistical segments, Z, in the network chains that are formed by chemical and physical network junctions:[58,60]

$$Z = (T_2^{pl})/[a(T_2^{rl})] \quad (3)$$

where a is a theoretical coefficient which depends on the angle between the segment axis and the inter-nuclear vector for the nearest nuclear spins at the main chains. For polymers containing aliphatic protons in the main chain, this coefficient is close to 6.2 ± 0.7.[60] T_2^{rl} is the relaxation time measured below T_g for the polymer swollen in a deuterated solvent. T_2^{rl} for swollen EPDM, as measured at –133 °C, is 10.4 ± 0.2 μs.[56] For calculation of the entanglement network in the amorphous phase of semicrystalline HDPS, T_2^{pl} in equation 3 is replaced by T_2^{net} and T_2^{am} relaxation times which are defined in Part 3.2. Using the number of backbone bonds in one statistical segment, designated as C_∞, the weight-average molar mass of network chains between chemical and/or physical junctions (in the present study average molecular weight between apparent chain entanglement, M_e) is calculated from the Z value:

$$M_w = ZC_\infty M_u/n \tag{4}$$

where M_u is the molar mass per elementary chain unit, and n is the number of backbone bonds in an elementary chain unit. Several studies have provided C_∞ value for polyethylenes in the range from 5.7 to 7.38 carbon-carbon backbones.[61,62,63,64,65] A mean C_∞ value of 7.0 was used in the present study. With decreasing M_n of HDPE's, the fluctuation of entanglement nodes (in discrete binary entanglements model) or the tube diameter (in the tube model) at the time scale of the NMR T_2 relaxation experiment (~ T_2 value) increases which causes larger overestimation of the M_e value as compared to HDPE with higher M_n.[38]

3. RESULTS AND DISCUSSION

3.1. Changes in Phase Composition and Chain Dynamics in the Melting Temperature Range. Three types of chain segments with largely different segmental mobility are observed in all samples in the melting temperature range:

[1] Low mobile chain segments in the crystalline phase and, possibly, a small amount of short chain loops with constrained mobility on the crystal surface – the crystal-amorphous interface (T_2^{cr} – relaxation component).

[2] Mobile chain segments which are characterized by the T_2^{net} relaxation time. The T_2^{net} value for all samples is in the range which is typical for cross-linked polymers at temperatures well above T_g^d.[56,57,66,67] Therefore, this relaxation component is assigned to network chains in the amorphous phase. The network chains are formed by chain entanglements and physical junctions due to anchoring of chain segments to polymer crystals.

[3] Highly mobile chain segments which are characterized by a long decay time (T_2^{def} – relaxation component). T_2^{def} value is typical for the relaxation of oligomers and unentangled chain segments with freer, faster, and nearly isotropic reorientation, which could be viewed as defects in the network of entanglements.[67,68]

The assignment of T_2^{net} and T_2^{def} relaxation components is supported by results for previously studied HDPE melts.[38] The T_2 relaxation decay of HDPE melts consists of faster and slower decaying parts, which largely originate from entangled chain segments and highly mobile disentangled chain-end segments - short and long T_2, respectively.[38] The relative intensity of a slowly decaying part increases with a decrease in molecular weight.[38,69] Similar results are obtained in the present study (Supporting Information, Part 2.2). Relative intensity of T_2 relaxation component with long decay time in polyethylene melts at 150 °C ($\%T_2^{long}$) is comparable to the relative intensity of the fraction of disentangled chain segments ($\%T_2^{def}$) which is determined at low crystallinity (Figure S7). Moreover, $\%T_2^{def}$ at low crystallinity is close to the percent of

disentangled chain-end segments which is estimated from the molecular weight distribution function of the studied HDPE's (see Supporting Information S2.2). Thus, the T_2^{def} relaxation components largely originates from the relaxation of low-entangled chain-end segments and low molecular weight chains - network defects which dilute entanglement network in the amorphous phase.

Melting of crystals results in an increase in the number of network chains and network defects and in the mobility of these chain segments (Figures 2, 3). In order to determine the structure of the physical network in the amorphous phase, T_2 decay is recorded as a function of time at different temperatures in the melting temperature range. These experiments provide information about time-temperature induced changes in crystallinity, the amount of network chains and network defects in the amorphous phase, as well as about chain motions in crystalline and amorphous phases. The longer T_2 value, the larger amplitude and/or frequency of chain motions are. As example, results for biHMHB sample are shown in Figure 3.

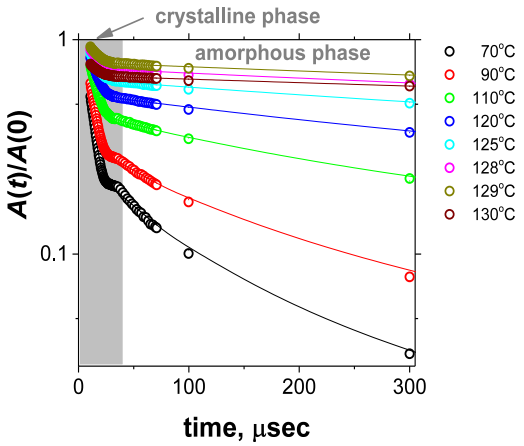

Figure 2a.

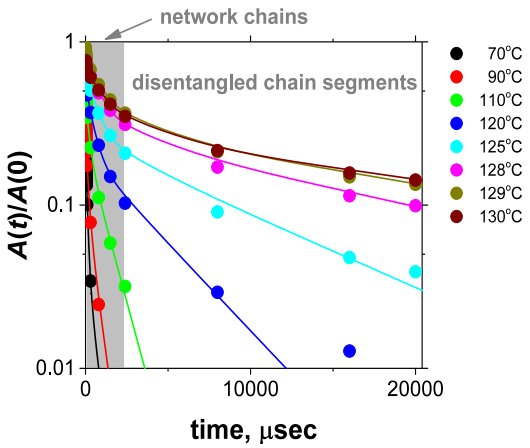

Figure 2b.

Figure 2. ^{1}H NMR T_2 relaxation decay at short (a) and long (b) decay time for the biHMHB sample in the melting temperature range. The decay was measured using SPE+HEPS experiment. The experiment was started five minutes after the NMR tube with the sample was placed in the NMR probe head, which was stabilized at the required temperature (Supporting Information S1.3). Lines show the results of the least-squares regression analysis of the decays using equation 2.

The effect of the dwelling time at different temperatures on the phase composition and chain mobility differs for different stages of the melting. At temperatures slightly higher than the onset of melting (e.g., above ≈ 100 °C for biHMHB), crystallinity slightly increases which is caused by lamellar thickening. A small decrease in crystallinity, which is followed by an increase is observed at the intermediate stage of melting, i.e., in the temperature range from approximately 120 to 125 °C for biHMHB. This initial decrease in crystallinity is caused by preferential melting of thinner crystals and/or less thermodynamically stable crystals. The partial melting is followed by recrystallization which results in an increase in crystallinity. The same behavior is observed for all HDPE samples studied. A similar conclusion can be drawn from the real-time WAXS measurements during isothermal annealing at 128 °C (see Figure 4, and Supporting Information, Figure S10). One can see that the initial drop of the WAXS crystallinity index at the moment when

the isothermal temperature is reached is followed by its gradual increase. At temperatures even closer to the end of melting, crystallinity exhibits only a decrease with time, which means that the recrystallization process becomes largely hindered at these high temperatures. The changes in crystallinity affect the chain mobility in the amorphous phase. The lower the crystallinity, the higher the mobility of chain segments in the amorphous phase, at all temperatures studied. The chain mobility in the crystals, which is characterized by the T_2^{cr} relaxation time, increases with increasing temperature due to the higher frequency of α-crystalline relaxation,[70,71,72] and with an increase in the size of the unit cell parameters of polymer crystals, as it was shown by WAXS studies,[73,74] thus increasing proton-proton distances and reducing the relaxation efficiency. However, close to the end of melting (at temperatures above 125 °C for biHMHB), the chain mobility in the crystals decreases. This means that only the most perfect and thermodynamically stable crystals with larger lamellae thickness survive until the end of melting. This interpretation is supported by SAXS data and by DSC study of annealing of samples in the melting temperature range which are described in Part 3.4 and in Supporting Information S3.2 and S4. SAXS data shows an increase in lamellar thickness during isothermal annealing in the final melting region (Supporting Information, Figure S9). A more detailed discussion of the X-ray experiments will be provided in a follow-up publication.

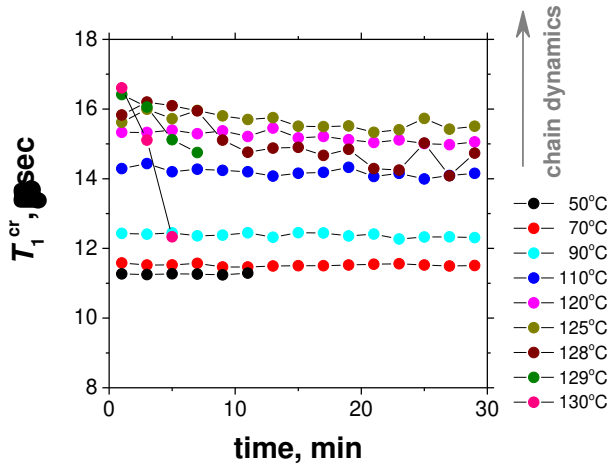

Figure 3a.

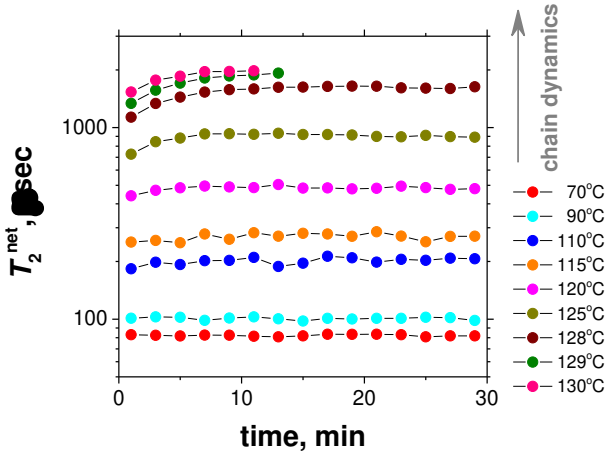

Figure 3b.

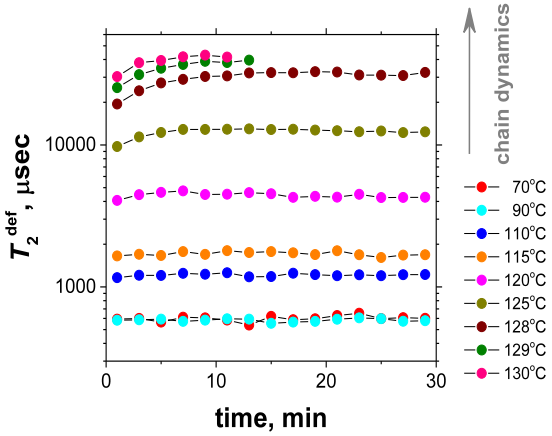

Figure 3c.

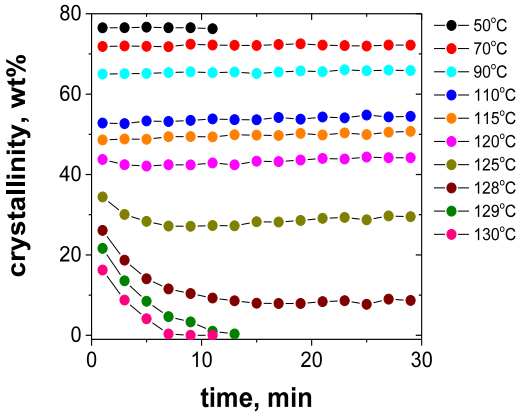

Figure 3d.

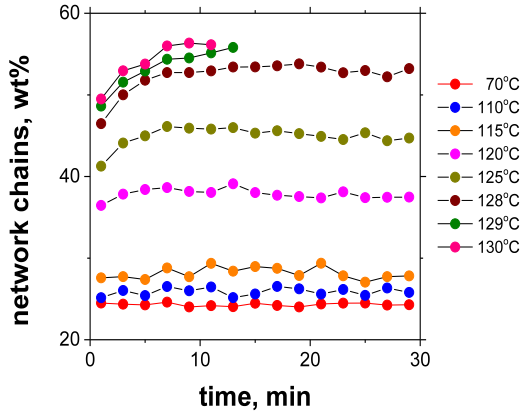

Figure 3e.

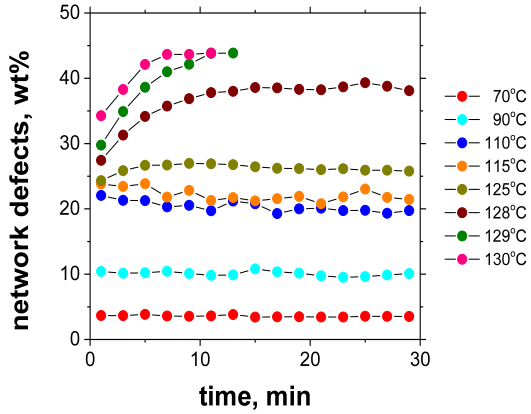

Figure 3f.

Figure 3. Dependence of the mobility of different types of chain segments as characterized by T_2^{index} - (a-c), crystallinity - (d), the amount of network chains - (e) and network defects - (f) in the amorphous phase against time at different temperatures for biHMHB.

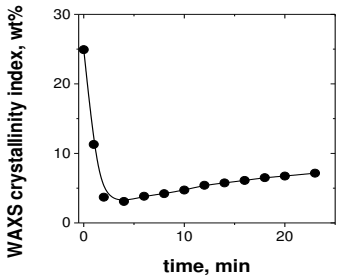

Figure 4. Time evolution of the WAXS crystallinity index of biHMHB during annealing at 128 °C.

3.2. Melting Behavior and the Structure of Physical Network in the Amorphous Phase.

At temperatures well above T_g, which in the case of the current PE's since the experiments are conducted in the melting temperature range, the T_2 relaxation time is a measure of the density of chain entanglements and junctions originating from the polymer crystals. The contribution of the polymer crystals to the total network density is the major component at temperatures below melting. Upon melting, the effect of polymer crystals decreases and chain entanglements provide a larger contribution to the total network density. At very low crystallinity, the value of T_2 can be used for the estimation of the entanglement density. It will be shown in Part 3.3 that no significant re-entangling occurs for high molecular weight HDPE in the melting temperature range due to the remaining crystals hindering chain reptation. Therefore, the evolution of the T_2 relaxation of the amorphous phase upon melting is studied for determining the entanglement density. The network structure in the amorphous phase is characterized by the following T_2 relaxation characteristics which are obtained by a least-squares fit of the T_2 decay (see equation 2): [1] The fraction of network chains and network defects in the amorphous phase which equals $f^{net} = A(0)^{net}/[A(0)^{net} + A(0)^{def}]$ and $f^{def} = A(0)^{def}/[A(0)^{net} + A(0)^{def}]$, respectively; [2] The T_2^{net} relaxation time; and [3] the population weight average T_2 relaxation rate of the amorphous phase, $1/T_2^{am}$, which is calculated as follows: $1/T_2^{am} = f^{net}/T_2^{net} + f^{def}/T_2^{def}$, where $f^{net} + f^{def} = 1$.

Care should be taken when interpreting the T_2 relaxation parameters in relation to the melting behavior due to several phenomena accompanying melting. A broad melting temperature range and several structural reorganizations are observed for semicrystalline polymers due to (1) the difference in the melting temperature of the crystalline polymorphs, (2) the difference in lamellar thickness, its size distribution and the crystal perfection, (3) the difference in the thickness of the interlamellar amorphous regions adjacent to the crystal; (4) the chemical structure variability such as the molecular weight distribution, the randomness of comonomers units and the stereoregularity, (5) the partial melting followed by recrystallization and the self-seeding effect, (6) the lamellar thickening and the crystal perfecting.[75,76,77,78,79,80,81] Although the temperature regulation of the NMR spectrometer is very accurate, the exact temperature within the sample volume is not known due to the endo- and exo-thermic processes accompanying melting and recrystallization. Moreover, a difference in heat transfer between randomly packed pieces of sample in the NMR tube adds to this uncertainty on the real temperature. This causes a deviation of the sample temperature from the temperature controller. Therefore, the extrapolation of the dependencies in Figure 3 to time zero would not provide an accurate value of the relaxation parameters at each temperature shortly after the expected temperature stabilization. In order to avoid this uncertainty in the data analysis, another approach is used. A similar approach has been previously used to determine the entanglement density in EPDM elastomers using a series of vulcanizates with a wide range of density of chemical crosslinks.[56] In order to determine the structure of the physical network, values of f^{net} and the T_2 relaxation rates $1/T_2^{net}$ and $1/T_2^{am}$ are plotted against crystallinity (Figures 5 and 6).

The fraction of network chains in high molecular weight R2 samples and nUHss increases with decreasing crystallinity (Figure 6). The increase can be explained by the formation of intra-lamellar amorphous gaps due to fragmentation of crystalline lamellae upon partial melting (Figure 7). The

melting process can start from the parts of the crystalline lamellae squeezed in the smallest amorphous gaps. [82] It can also first occur at the borderlines delimiting parts of the crystal grown from different secondary nuclei that can be observed in some instances by TEM dark-field imaging.[83] This causes the formation of additional network chains which interconnect fragmented crystalline lamellae. At lower temperatures, these chain segments feature a low mobility and contribute to the amount of the rigid polymer fraction - NMR crystallinity.[84] However, the fraction of network chains in the amorphous phase decreases upon melting of both the bimodal and R1 samples. It is suggested that fragmentation of crystal lamellae occurs in the proximity of chain ends. The release of chain ends causes the decrease in the number of physical junctions which originate from the polymer crystals and an increase in the number of disentangled chain-end segments as shown on schematic drawing on Figure 7.

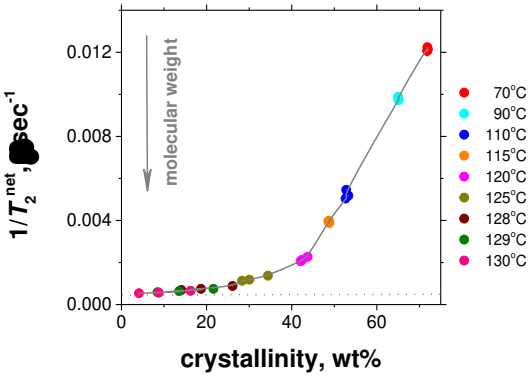

Figure 5a.

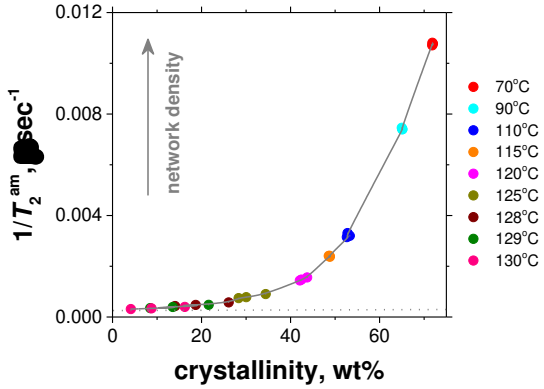

Figure 5b.

Figure 5. The relaxation rate $1/T_2^{net}$ – (a) and $1/T_2^{am}$ – (b) plotted against crystallinity which is determined as a function of time at different temperatures for the biHMHB sample. Arrows indicate change in (a) molecular weight of network chains; and (b) - network density which is composed of physical junctions from polymer crystals and chain entanglements. Only the data points, which are recorded during 2 – 4 minutes after the sample reaches the required temperature, are used for these plots.

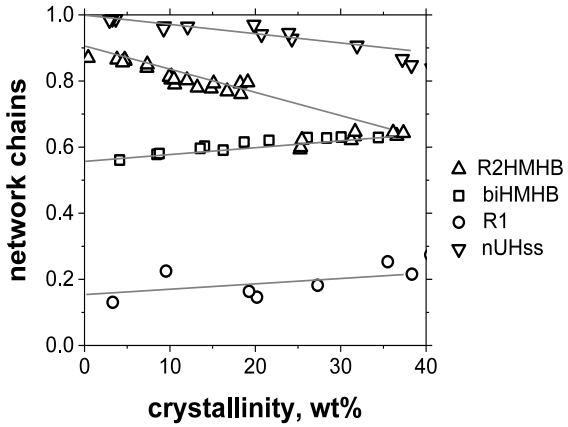

Figure 6. The fraction of network chains f^{net} in the amorphous phase plotted against crystallinity which is determined as a function of time at different temperatures for R2HMHB, biHMHB, R1 and nascent UHMPE powder (nUHss).

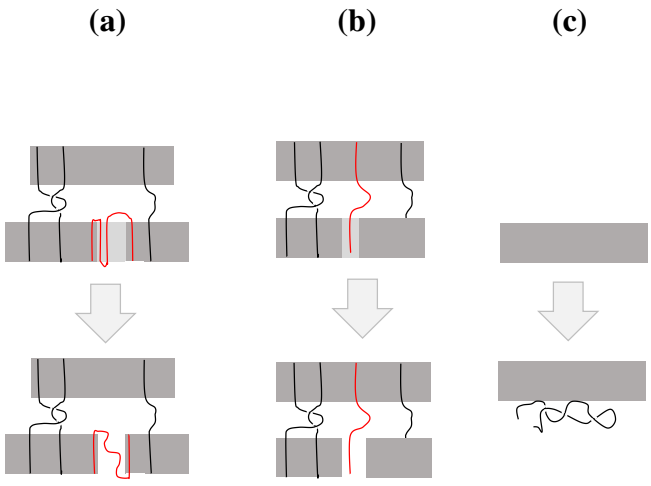

Figure 7. Schematic drawing which shows the effect of partial melting on the number of network chains in the amorphous phase of high - (a) and low molecular weight – (b) polyethylenes which are melt-crystallized; and in hpc-HDPE – (c). Light grey areas on the upper drawings show lamellar fragments which melt at lower temperatures than the rest of the lamellae. Such local melting point depression can be accounted by the fact that these lamellar fragments are squeezed in the smallest amorphous gaps or contain grain boundaries.

3.3. Chain Entanglements in the Amorphous Phase of Polyethylene's. The density of physical junctions from polymer crystals decreases upon melting which causes a large decrease in the relaxation rates $1/T_2^{net}$ and $1/T_2^{am}$ (Figure 5). In addition to that, the volume average density of chain entanglements in the amorphous phase, which are trapped by crystals, decreases due to the increase in the amount of amorphous phase upon melting. The dependencies reach an asymptotic constant value at a crystallinity below 10 wt.%. The values of $1/T_2^{net}$ and $1/T_2^{am}$ extrapolated to zero crystallinity are used for calculating the weight average molecular weight of chain segments between apparent chain entanglements, M_e, and the average entanglement density, $1/2M_e^{am}$, respectively, using equations 3 and 4. The following assumptions are made for quantifying the entanglement network in the amorphous phase. (1) A significant fraction of the lamellar crystals remains intact upon partial melting during 2 – 4 minutes. The remaining crystals keep the pre-existing entanglement network largely intact. (2) Topological constraints from the remaining crystals in molten domains – the so called "corset effect"[85] – are negligibly low. (3) Chain reptation does not cause a significant change in the entanglement density upon approaching the end of melting.

(1). The fraction of crystals which remains intact upon partial melting is estimated by DSC. DSC thermograms are compared for samples at first heating and after the consequent isothermal

steps in the melting temperature range followed by sample cooling to room temperature. A new sample was taken for the experiments at each annealing time and each annealing temperature. The consequent isothermal steps in the DSC experiments were the same as those used for the NMR experiments (see Supporting Information S3.2). A single broad melting endotherm is observed at the first heating. Two melting endotherms are observed after the annealing of samples in the melting temperature range, followed by cooling and reheating. The first melting peak is observed at approximately the same temperature as for the samples before annealing. The enthalpy of melting for this peak decreases with increasing time of isothermal annealing and it is lower at higher annealing temperature. The second melting peak is observed at a higher temperature. The enthalpy of melting corresponding to this second endotherm increases with increasing annealing time and temperature. The melting peak at lower temperature is assigned to crystals which are formed from the molten fraction of HDPE after cooling. The melting peak at the higher temperature originates from unmolten remnant crystals. The higher melting temperature of the unmolten crystals is due to lamellar thickening and crystal perfection during annealing. This fraction of unmolten crystals decreases with increasing annealing time and temperature. As evidenced by DSC (see Supporting Information S 3.2), approximately 5 – 10 wt. % of the crystals remain unmolten during the 2 – 4 minutes annealing at temperatures close to the end of melting. It should be noted that the estimated fraction of unmolten crystals suffers from uncertainty due to the complexity of phenomena which occur upon partial melting as discussed above. Regardless of these phenomena, as will be discussed below, a complete reptation (re-entangling) of the chain is slowed down by the remaining and newly formed crystals since chain diffusion through crystals has to be accompanied by a local chain elongation and this is consequently restricted by the concomitant additional entropic force.

(2). The topological constraints from the remaining crystals in the molten domains – the so called "corset effect"[85] - can cause higher anisotropy of the chain motions. This will result in a lower calculated M_e value. The thickness of the amorphous layer between the surface of adjacently stacked crystal lamellae is 3 - 3.5 nm at temperatures below the melting of HDPE without branches.[45] This value is smaller than or comparable to the typical tube diameter in HDPE melts, i.e., d = 6 and 4.87 nm for PE with M_w = 12.4 and 190 kg/mol, respectively.[86] A molecular dynamics study reported the tube diameter to be in the range from 3.2 to 4.5 nm.[87] Therefore, the chain segments in the amorphous domains reside in a largely confined geometry at temperatures below the onset of melting.

The thickness of the crystal lamellae, of the amorphous interlamellar regions and of the long period are computed from the time- and temperature-resolved SAXS experiments carried out with a time-resolution of 6 s. The results corresponding to a heating ramp of 10.0 °C/min are shown in Figure 8, and in Figure S11 in Supporting Information. Upon heating, the thickness of the crystalline lamellae decreases due to the surface melting phenomenon,[88] while the interlamellar amorphous regions consequently increases in thickness. This is in line with previous observations[89] in which the crystals confined in the smallest amorphous gaps were found to melt first. At a WAXS crystallinity of about 35 %, the thickness of the crystalline and the amorphous regions become equal. Extrapolation of the dependence to crystallinity values of 5 – 10 wt. % provides the average distance between adjacent lamellae. Its value is at least two times larger than the typical tube diameter. Therefore, "the corset effect" should not cause a large increase in anisotropy of segmental motion in the amorphous phase at low crystallinity. This conclusion is also confirmed by the following results. If "the corset effect" would be the determining factor, the apparent M_e value should be similar at the same crystallinity for all samples. However, M_e increases with a decrease of M_n as it will be shown below. Thus, the values of $1/T_2^{net}$ and $1/T_2^{am}$ can be used for calculating

the weight average molecular weight of chain segments between apparent chain entanglements, M_e, and the average entanglement density, as described in Part 2.8. It should be noted that the distribution of chain entanglements in high molecular weight semicrystalline polymers is heterogeneous in space since most of the entanglements cannot be disentangled during rapid crystallization and preexisting entanglements in the melt are pushed to the inter-lamellar layers by the growing crystals.[90,91,92] Since no significant re-entangling occurs upon melting of high molecular weight HDPE, entanglement density in the amorphous phase below melting temperatures can be estimated from the known amount of the amorphous phase. The present experiments cannot detect this heterogeneous distribution of chain entanglements, since T_2^{net} provides a weight average molecular weight between apparent chain entanglements, M_e.

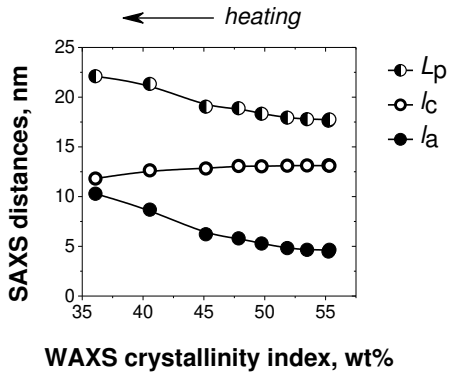

Figure 8. Values of crystalline lamellar thickness - l_c, interlamellar amorphous region thickness – l_a, and long period - L_p for the biHMHB sample as a function of the WAXS crystallinity index measured during a heating ramp of 10.0 °C/min.

(3). As was shown above, approximately 5 – 10 wt. % of the crystals remain unmolten during the 2 – 4 minutes annealing at temperatures close to the end of melting. To completely prevent chain reptation in partially molten HDPE each chain should be attached at least to one or two crystals. The typical lamellar thickness of melt-crystallized HDPE is approximately 15 nm.[45] Given

the chain tilt of the stems with respect to the lamella normal, such lamellae are formed by chain stems consisting of approximately 146 CH_2 units.[93] The molecular weight of such chain segments is 2044 g/mol. Taking into account that 5 – 10 wt. % of crystals remain unmolten during 2 – 4 minutes at temperatures close to the end of melting, the majority of the HDPE chains with a molecular weight above $\approx (20 - 40)\cdot 10^3$ g/mol will be still attached to one or more crystals. The reptation of chains with a lower molecular weight cannot be excluded. An increase in volume upon melting might also influence entanglement density. Nevertheless, the re-entanglement process in the molten fraction is rather slow as suggested by several studies.[92,94,95] Moreover, the mean-squared end-to-end distance of polymer chains with $M_n > (20 - 40)\cdot 10^3$ g/mol is larger than the thickness of interlamellar layers at the end of melting as determined by SAXS (Figure 8), which largely reduces probability of re-entangling and chain reptation. Therefore, it can be concluded that re-entanglement in the amorphous phase of partially molten HDPE's will be negligible. It is noted that contrary to HDPE melts the remaining crystals at the end of melting suppress fluctuations of entanglement knots as it follows from comparison of T_2 values, which are measured at the same temperature for the amorphous phase (T_2^{am}) and molten HDPE's (T_2^{melt}). Values of (T_2^{melt}) larger than T_2^{am} (Supporting Information, S2.3). Fluctuation of entanglement knots in HDPE melts doesn't allow using values of T_2 for HDPE melts for determining M_e using equation 4.

The conclusion above that the remaining crystals largely prevent re-entanglement in partially molten high molecular weight HDPE's is supported by studies of the melting behavior of hpc-HDPE and the same melt-crystallization sample (mc-HDPE). The fraction of network chains, f^{net}, for mc-HDPE increases with decreasing crystallinity similar to that for R2HMHB and nUHss, as it is shown in Figure 6, and approaches 0.78 at low crystallinity. f^{net} for hpc-HDPE does not depend on crystallinity and equals 0.78 ± 0.02. Such behavior should correspond to the consecutive

detachment of chains from the crystal surface with the formation of molten surface layer (Figure 7). One would expect a faster chain reptation in the molten surface layer of hpc-HDPE than in the amorphous phase of mc-HDPE where physical junctions from polymer crystals prevent reptation. However, mc-HDPE shows a change in $1/T_2^{am}$ against crystallinity similar to that for the other melt-crystallized HDPE's (see Figure 9), whereas $1/T_2^{am}$ for hpc-HDPE is lower than for mc-HDPE even at a crystallinity approaching zero and its value hardly changes with crystallinity. The smaller value of $1/T_2^{am}$ for hpc-HDPE is due to the lower entanglement density in the molten part of hpc-HDPE. This means that the re-entanglement process in the amorphous domains of hpc-HDPE is rather slow despite [1] the lower number of constraints on chain diffusion (reptation) than for mc-HDPE (Figure 7), and [2] the short reptation time for HDPE with similar molecular weight, i.e., approximately 1 – 2 sec.[96] A small increase in $1/T_2^{am}$, which is observed with decreasing crystallinity (Figure 9), is caused by a rather slow chain reptation in the molten domains which increases the entanglement density. Therefore, it can be concluded that chain reptation during 2 – 4 minutes in the melting temperature range can be largely excluded for melt-crystallized HDPE's with high molecular weight.

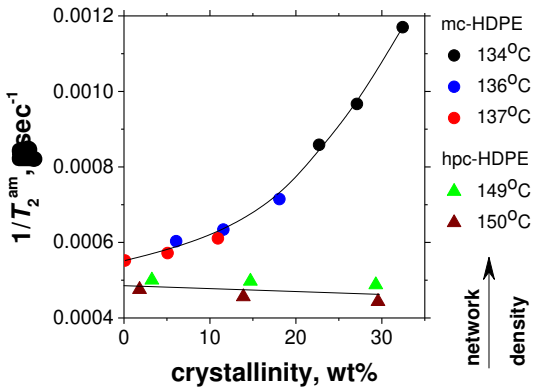

Figure 9. Dependence of $1/T_2^{am}$ against crystallinity which is determined as at different temperatures with time interval of 2 min at each temperature for hpc-HDPE and the same melt-crystallized polymer – mc-HDPE.

3.4. Molecular Weight Between Chain Entanglements as Determined by Different Methods. For a large variety of polymers, molecular weight between chain entanglements is the most studied for polyethylenes using different methods. There is large variation in both the computational and experimental estimates of M_e for PE. Computer simulations provide M_e values ranging from 492 to 840 g/mol.[97,98] Recent time-domain NMR experiments determined apparent M_e of 1760 g/mol.[38] A typical M_e value of 1250 g/mol is commonly accepted by rheologists. However, previous rheological studies provided M_e values in the range from 828 to 2600 g/mol.[99,100,101]

The large discrepancy in the M_e values has several causes, i.e., (1) the different molecular architecture of the PE's studied, namely: M_w, molecular weight distribution (MWD) and the presence of short- and long-chain branches; (2) the difference in the time- and length-scales of chain dynamics as probed by different methods; (3) several methodological issues, experimental artifacts, assumptions of theories which are used for calculation of M_e values from measured characteristics of entanglement density.[26,102,103,104,105] Despite numerous studies, theories which are used for calculating M_e from rheological data rely on several assumptions, as it was highlighted by several researchers. The following conclusions were stated based on molecular dynamic (MD) simulations of entangled polymer melts. "We do not think that determining the number of entanglements or N_e is a well-defined task worth pursuing. Instead, one must search for a better model and then seek to determine its parameters from MD".[102] Likhtman states in another publication that "we do not believe that counting entanglements is meaningful without having a reliable model which can use this number to predict all dynamic properties".[103] Milner made the following comment on the tube model. "The tube [model] itself is an intuitively appealing concept that remains somewhat elusive".[26] Based on theoretical analysis of the viscosity of polymeric

liquids Doi concluded that "the interpretation of the chain-end influence on the stress relaxation modulus is rather descriptive in that it serves as "diluent" of the entangled fraction".[106]

As far as time-domain NMR is concerned, the NMR T_2 relaxation method is also not free from assumptions. The method measures the time average of anisotropy of segmental motion in the time window of ~1 - 10 ms over the whole sample. The assumption of fixed network junctions and constraints from chain entanglements, which is made in NMR theories,[58,69] is not quite correct. Entangled nodes (in the discrete entanglement model) or the tube diameter (in the tube model) fluctuate on the time scale of the NMR experiment, thus reducing the strength of the dipolar interactions. Therefore, the lower M_n, the larger the overestimation of NMR value of M_e is. It should be noticed that estimated by NMR M_e value for UHMWPE (1760 g/mol)[38] is in the range of M_e determined by previous rheological studies, i.e., from 830 to 2600 g/mol.[99,100,101]

3.5. The Effect of Molecular Structure on Density of Apparent Chain Entanglements in the Amorphous Phase as Determined by the NMR Method. The characteristics of the network structure in the amorphous phase of HDPE samples at crystallinity approaching zero are provided in Table 3. Two types of segmental motions are observed at low crystallinity, i.e., the anisotropic motion of entangled chain segments which is characterized by the T_2^{net} value, and fast, nearly isotropic reorientation of the disentangled chain-end segments responsible for the T_2^{def} relaxation. The fraction of disentangled chain-end segments, which equals approximately $4M_e/M_n$,[38,69] increases with decreasing M_n (Supporting Information, S2.2, Table S3). Despite the more simplified analysis of the T_2 decay shape of the amorphous phase from only eight data points, the value of the apparent M_e for nUHss is the same as for ultra-high molecular weight PE which was determined using a theoretical analysis of the shape of the T_2 relaxation decay in the melt at 150 °C, namely 1760 ± 80 g/mol.[38,107,108] The value of the apparent M_e of the entangled chain segments

increases with decreasing M_n as it was shown previously.[38,69] The effect is the most pronounced for bimodal HDPE's which contain a significant fraction of low-molecular weight R1 HDPE (M_n = 3.6 kg/mol). This observed increase is caused by a decrease in the confinement on the mobility of entangled chain segments due to solvent-like dilution of the entanglement network by highly mobile chain-end segments and low molecular weight chains.[106,109,110,111] Polymer crystals hinder re-entanglement in the melting temperature range as it was discussed above. As far as the entanglement density in the amorphous phase below the melting temperature is concerned, growing crystals push entanglements into the amorphous phase that decreases in volume with crystal growth. Therefore, the density of the apparent chain entanglements in the amorphous phase increases with crystallinity increase, and its value below the onset of melting is approximately two times larger (for a crystallinity of ~ 50 %) as compared to that at crystallinity approaching zero. This agrees with results of recent study.[91]

3.6. Density of Apparent Chain Entanglements in Relation to the Mechanical Properties. On a microscopic scale failure mechanisms of polyolefins are known to be determined by several *interrelated* physical structure characteristics i.e.: (1) chain entanglements; (2) the density of tie molecules - chain segments which interconnect adjacent crystals and keep the crystalline and amorphous domains from separating under load; (3) the ability of this tie molecular chain network to redistribute local forces on chain segments after a load was applied, and to decelerate further chain slippages through the semicrystalline morphology; (4) crystallinity and crystal thickness; (5) the chain mobility in the crystalline and the amorphous phases; and (6) possibly some other factors. Although very valuable for understanding the morphological changes, this microscopic view cannot be directly used to describe and predict failure mechanisms. To that end, a meso-scale description is used in which all of the above characteristics are reduced to a homogeneous network

of loaded chains, leading to a time and temperature dependent surface energy, that directly determines the propensity to brittle failure via craze propagation.[112,113] The available network of entanglements at the time and temperature scales of a mechanical experiment determines the failure mechanisms that will occur, such as ductile failure by shear yielding or craze propagation leading to brittle failure via a craze-crack mechanism.[22,112,114,115,116] An extra complication lies in the fact that the morphology and the remnant network of entanglements change upon deformation, and not all entangled chains can form load bearing tie molecules. However, it turns out that mechanical observables in the strain hardening regime provide valid estimates of the active network that determines the resistance to long-term failure. Such observables are the strain hardening modulus $\langle G_p \rangle$, the natural draw ratio and the creep rate deceleration factor.

Table 3. The Structure of the Entangled Network in Amorphous Phase of HDPE Samples at Crystallinity Value Approaching Zero.*

Sample	f^{net}, wt.%	$1/T_2^{net}$, ms^{-1}	M_e, g/mol	$1/T_2^{am}$, ms^{-1}	$1/2M_e^{am}$, mmol/kg
biHMHB	54	0.52	2920	0.29	95.5
biHMLB	55	0.53	2870	0.31	102
biLMHB	50	0.45	3370	0.24	79.5
biLMLB	51	0.48	3160	0.26	86.1
R2HMHB	89	0.70	2180	0.68	224
R2HMLB	90	0.70	2180	0.68	224
R2LMHB	82	0.70	2180	0.59	194
R2LMLB	82	0.73	2080	0.65	214
R1	16	0.20	7630	0.035	11.5

nUHss	100	0.88	1730	0.88	288
mc-HDPE	78	0.70	2520	0.57	198

* f^{net} is the weight fraction of entangled chain segments. $1/T_2^{net}$ is the relaxation rate of entangled chain segments. M_e is the weight average molecular weight of chain segments between apparent chain entanglements nodes. $1/T_2^{am}$ is the relaxation rate of the amorphous phase composed of entangled chain segments and the highly mobile low-entangled chain-end segments. $1/2M_e^{am}$ is the volume average density of apparent chain entanglements assuming that entanglements are binary contacts between chains. The estimated absolute error in % network chains is 3 wt.%. The estimated relative error of $1/T_2$ values is 10 %. M_e for hpc-HDPE is significantly larger than for mc-HDPE. However, the network characteristics for hpc-HDPE are not determined due to the partial re-entanglement during melting.

Resistance of HDPE to creep, which is characterized by the CRDF, is determined for bimodal and R2 HDPE samples with different molecular weight characteristics and the amount of ethyl branches (see Table 1). Increase in the molecular weight and, consequently, the average number of effective chain entanglements cause significant improvement of the CRDF (Figure 10). The effect of molecular weight on the entanglement network is shown in Figure 11. The distinct difference in $1/T_2^{am}$ for HDPE's with a different molecular weight is caused by the chain-end segments. The CH_3 groups at the end of polymer chains mainly reside in a nearly solid-like environment in the amorphous domains.[49] The chain ends dilute the entanglement density in the amorphous phase and increase the segmental mobility. The average density of physical junctions at the same crystallinity is larger for HDPE with a higher molecular weight. Consequently, the maximum possible number of network chains that are able to bear load increases with an increase in molecular weight (Table 3). In addition to a higher effective entanglement density longer chains will interconnect more

lamellae and cause a larger resistance for the chain to slip through the crystals. This slows down the disentanglement of molecules and, consequently, prevents a decrease in the number of tie molecules.[18]

The HDPE's with similar molecular weight and higher branching content feature better creep resistance as it was recently shown.[116] The effect is small for HDPE's with a low molecular weight due to the low fraction of effective network chains. The effect of chain branches on CRDF is the most pronounced for HDPE's with a high molecular weight. An increase in the number of short-chain branches causes a crystallinity decrease, an increase in the amount of rubbery-like fraction in the amorphous phase and an increase in segmental mobility in the amorphous phase (Supporting Information, Table S1). It can be suggested that *at the initial stage of deformation* a higher segmental mobility in the amorphous phase - lower molecular friction coefficient - is in favor of redistributing (equalizing) local forces exposed to tie molecules upon loading. Since coupling of chain motions in both phases is required, diffusion of overloaded tie chains would be faster for more mobile chain segments in the amorphous phase. This suggestion is supported by results of the following studies. Loading of network chains is very heterogeneous for HDPE which is stretched at 70 °C.[117] An NMR study of strain-recovered isotactic polypropylene (iPP) has shown that stretching at room temperature induces imperfections in crystalline domains, whereas deformation at higher temperatures causes a crystallinity increase, an increase in crystal thickness and a decrease in molecular mobility in crystalline and amorphous domains.[118] A DMTA study of PE has shown that higher segmental mobility in the amorphous phase facilitates fibrils formation. As result of that, the material is less deformed and is able to sustain a lower stress for a longer time.[119] These results support our conclusion that higher segmental mobility in the amorphous phase enhances the time resilience of the tie molecular network.

The other structural characteristic of HDPE's, which determines the CRDF, is the number of short-chain branches. A small fraction of ethyl branches is trapped within the crystals.[120,121] Branches within crystals cause local crystal disorder which can initiate fragmentation of lamellae with the formation of additional network chains, as shown on the schematic drawing in Figure 7. Lamellar fragmentation can also reduce local forces. Lamellar thickness is lower at higher number of branches and as consequence the tie molecular network will be denser.[18] In a course of redistribution of local forces on tie molecules, chain branches slow down chain diffusion through crystals due to the increase in activation energy required for this process. This reduces further displacing of molecules in the semicrystalline morphology and improves the long-term resilience of the tie molecules and hence creep related properties.[122]

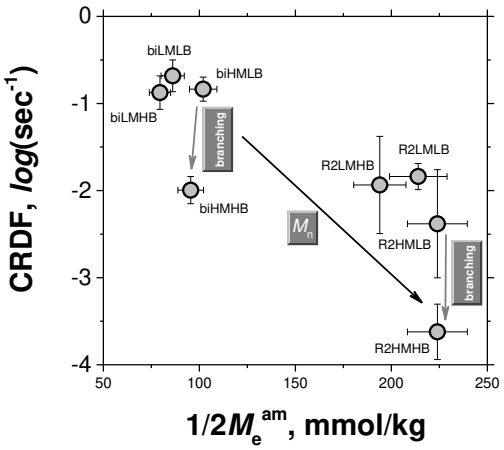

Figure 10. Creep rate deceleration factor against apparent entanglement density. The arrows show the effect of ethyl branches and M_n on CRDF.

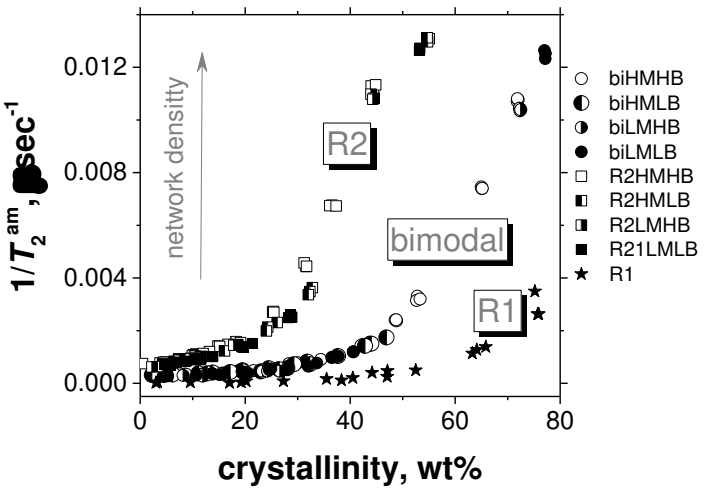

Figure 11. Relaxation rate in the amorphous phase against crystallinity for R1, R2 and bimodal HDPE's.

4. CONCLUSIONS

The density of chain entanglements in the amorphous phase of semicrystalline polymers and the number of tie molecules are important characteristics, which determine the deformation and failure mechanisms in long-term tests like creep. However, direct estimation of the entanglement network in semicrystalline polyolefins is still an unresolved issue. A methodology for estimating the apparent entanglement density in the amorphous phase of semicrystalline polyolefins was developed. The method is based on the analysis of the density of the physical network junctions in the amorphous phase by ^{1}H NMR T_2 relaxation analysis. This method was already widely used for the analysis of the density of chemical crosslinks and chain entanglements in amorphous viscoelastic materials,[37,38,55,56,66,67] and rubbery phases in polymer blends.[67, 123] The same methodology cannot be directly implemented for the estimation of the entanglement density in the amorphous phase of semicrystalline polymers because NMR T_2 relaxation time of the amorphous phase is affected not only by chain entanglements but also by the presence of crystals. Moreover, polymer crystals impose constraints on translational chain motions in the amorphous phase which

also affect the T_2 value. In order to reduce the effect of physical junctions from polymer crystals, the T_2 relaxation analysis was performed at temperatures close to the end of melting. In the limit of vanishing crystallinity, the chain entanglements provide the major contribution to the T_2 relaxation time of the amorphous phase. The NMR measurements are complemented by synchrotron time- and temperature-resolved SAXS/WAXS experiments, which allowed the determination of the values of crystallinity and length scales of the semicrystalline structure evolution upon melting.

In order to avoid changes in the entanglement density which can be caused by chain reptation in the amorphous domains upon melting, the NMR T_2 relaxation experiment was optimized for fast recording the decay of the transverse magnetization relaxation (T_2 decay) from both the crystalline and the amorphous domains without a significant loss in the accuracy as compared to experiments with longer measuring times. The T_2 decay was recorded *as a function of time at different temperatures* in the melting temperature range. Analysis of the T_2 decay provided quantitative information on melting-induced changes in the phase composition and the chain mobility in the crystalline and the amorphous phases. The following melting-induced phenomena in semicrystalline polymers are observed: (1) An annealing effect at temperatures slightly above the onset of melting; (2) a partial melting followed by recrystallization at higher temperatures; and (3) a continuous decrease in crystallinity at temperatures close to the end of melting. In all cases, the decrease in crystallinity causes an increase in chain mobility in the amorphous phase. The network structure in the amorphous phase consists of contributions from the entangled network chains and the highly mobile network defects, i.e., dangling chain-end segments, low-entangled chain segments and, possibly, chain segments rich in comonomers units. The fraction of network chains increases with decreasing crystallinity for high molecular weight polyethylene. This is explained by partial melting of crystalline lamellae with the formation of network chains in intra-lamellar

amorphous gaps.[82] These additional network chains interconnect fragmented crystal lamellae. Contrary to high molecular weight HDPE, the fraction of network chains decreases upon melting of HDPE samples with lower M_n. This may suggest that lamellar fragments with adjacent chain ends melt at lower temperatures than those formed by the middle part of chains.

At temperatures close to the end of melting, the contribution of crystals to the physical network in the amorphous phase diminishes, which allows the estimation of the remnant entanglement network. It was shown that the residual crystallinity largely prevents chain reptation thus preserving the average entanglement density in high molecular weight HDPE's. Therefore, the entanglement density in the amorphous phase below the melting temperatures can be estimated from the known amount of amorphous phase. The network density is characterized by: (1) the fraction of entangled network chains, f^{net}; (2) the weight average molecular weight of network chains between apparent chain entanglements, M_e; and (3) the volume average density of apparent chain entanglements, $1/2M_e$. The volume average structure of the network of entanglements was estimated in a series of HDPE samples with largely different molecular weight characteristics and with different comonomer content. The molecular weight influences the density of the entanglement network as determined by the currently presented NMR method. The fraction of entangled chain segments decreases with decreasing M_n due to the increasing fraction of disentangled chain-end segments. The value of the apparent M_e increases with decreasing M_n as it was shown previously due to a dynamic "dilution" effect of un-entangled chain-end segments.[38,69] The apparent M_e is larger for all samples than its limiting value for ultra-high molecular weight PE which equals 1760 ± 80 g/mol.[38]

The methodology developed in this study is of interest for determining the effect of crystallization conditions, processing conditions and the molecular structure on phase composition, melting behavior and chain entanglements in amorphous phase of polyolefins. The method allows

also to quantify the fraction of entangled network chains which potentially can form tie chain segments during deformation. Knowledge of the potentially available entanglement density allows the ranking of materials with respect to network dependent properties such as creep failure due to slow crack growth.[22] Hitherto, mechanical methods that are heavily dependent on geometry and precision of dimensions were used to characterize this effective network. Thanks to the NMR method presented in this paper such complications can be avoided since results of the method do not depend on the shape of the sample and can even be measured on a powder sample.

Both a larger number of ethyl branches and a higher molecular weight are in a favor of resistance of HDPE to creep failure. The role of the molecular weight characteristics such as polydispersity, the type of chain branches, their number and distribution between long and short chains will be topic for our further study.

ASSOCIATED CONTENT

Supporting Information

The Supporting Information is available free of charge on the ACS Publications website at DOI. The following results are presented: (1) tensile creep tests; (2) NMR methods and optimization of NMR T_2 relaxation experiments for fast recording of T_2 decay in melting temperature range; (3) T_2 relaxation for the amorphous phase at the end of melting and for the melt; (4) the fraction of disentangled chain-end segments which is calculated from molecular weight distribution function of the studied HDPE's; (5) thermal analysis of samples by DSC; (6) synchrotron X-ray analysis.

AUTHOR INFORMATION

Corresponding Author

*E-mail: v.lit.con@kpnmail.nl

Notes

The authors declare no competing financial interest.

AKNOWLEDGEMENTS

The authors thank Dr. Miguel Cordova from Sabic Technology and Innovation for performing DSC experiments, and Dr. Arnold Wilbers from DSM-DMSC for calculation of the fraction of disentangled chain end segments. We are indebted to Prof. Dr. I. M. Ward from University of Leeds for continuously challenging and supporting the concept of a resilient network of tie molecules and its relevance for creep response and failure. VL acknowledged permission of DSM Resolve for using the Minispec MQ20. Our special thank goes to Prof. G. W. M. Peters from Technical University of Eindhoven who provided us with high pressure crystallized HDPE. Dimitri Ivanov thanks financial support from RFBR, project number 19-29-12049. His work was done on the theme of state task № 0074-2019-0014 (registration № AAAA-A19-119101590029-0).

REFERENCES

[1] Ward, I. M.; Sweeney, J. *Mechanical Properties of Solid Polymers*; 3rd ed.; John Wiley & Sons, Ltd.: Chichester, 2012.

[2] Nwabunma, D.; Kyu, T., Eds.; *Polyolefin Blends*; Wiley-Interscience, John Wiley & Sons, Inc. Publication: Hoboken, New Jersey, 2008.

[3] Bubeck, R. A.; Baker, H. M. The influence of branch length on the deformation and microstructure of polyethylene. *Polymer* **1982**, *23*, 1680-1684.

[4] Huang, Y. -L.; Brown, N. Dependence of slow crack growth in polyethylene on butyl branch density: Morphology and theory. *J. Polym. Sci.: Part B: Polym. Phys.* **1991**, *29*, 129-137.

[5] Ohta, Y.; Yasuda, H. The influence of short branches on the α, β and γ relaxation processes of ultra-high strength polyethylene fibers. *J. Polym. Sci.: Part B: Polym. Phys*. **1994**, *32*, 2241-2249.

[6] Rasburn, J.; Klein, P. G.; Ward, I. M. The influence of short-chain branching on the creep behavior of oriented polyethylene, and its effect on the efficiency of crosslinking by electron irradiation, *J. Polym. Sci.: Part B: Polym. Phys*. **1994**, *32*, 1329-1338.

[7] Ohta, Y.; Suciyama, H.; Yasuda, H. Short branch effect on the creep properties of the ultra-high strength polyethylene fibers. *J. Polym. Sci.: Part B: Polym. Phys*. **1994**, *32*, 2241-2249.

[8] Brooks, N. W. J.; Duckett, R. A.; Ward, I. M. Temperature and strain-rate dependence of yield stress of polyethylene. *J. Polym. Sci.: Part B: Polym. Phys.* **1998**, *36*, 2177-2189.

[9] Hiss, R.; Hobeika, S.; Lynn, C.; Strobl, G. Network strength, slip processes and fragmentation of crystallites during uniaxial drawing of polyethylene and related copolymers. A comparative study. *Macromolecules* **1999**, *32*, 4390-4403.

[10] Hubert, L.; David, L.; Séguéla, R.; Vigier, G.; Degoulet, C.; Germain, Y. Physical and mechanical properties of polyethylene for pipes in relation to molecular architecture. I. Microstructure and crystallisation kinetics. *Polymer* **2001**, *42*, 8425-8434.

[11] O'Connell, P. A.; Bonner, M. J.; Duckett, R. A.; Ward, I. M. Effect of molecular weight and branch content on the creep behavior of oriented polyethylene. *J. Appl. Polym. Sci.* **2003**, *89*, 1663-1670.

[12] Gupta, P.; Wilkes, G. L.; Sukhadia, A. M.; Krishnaswamy, R. K.; Lamborn, M. J.; Wharry, S. M.; Tso, C. C.; DesLauriers, P. J.; Mansfield, T.; Beyer, F. L. Does the length of the short chain branch affect the mechanical properties of linear low density polyethylenes? An investigation based on films of copolymers of ethylene/1-butene, ethylene/1-hexane and ethylene/1-octene synthesized by a single site metallocene catalyst. *Polymer* **2005**, *46*, 8819-8837.

[13] Bartczak, Z.; Kozanecki, M. Influence of molecular parameters on high-strain deformation of polyethylene in the plane-strain compression. Part I. Stress-strain behavior. *Polymer* **2005**, *46*, 8210-8221.

[14] Cazenave, J.; Seguela, R.; Sixou, B.; Germain, Y. Short-term mechanical and structural approaches for the evaluation of polyethylene stress crack resistance. *Polymer* **2006**, *47*, 3904-3914.

[15] Krishnaswamy, R. K.; Yang, Q.; Fernandez-Ballester, L.; Kornfield, J. A. Effect of the distribution of short-chain branches on crystallization kinetics and mechanical properties of high-density polyethylene. *Macromolecules* **2008**, *41*, 1693-1704.

[16] Nozue, Y.; Kawashima, Y.; Seno, S.; Nagamatsu, T.; Hosoda, S.; Berda, E. B.; Rojas, G.; Baughman, T. W.; Wagener, K. B. Unusual crystallization behavior of polyethylene having precisely spaced branches. *Macromolecules* **2011**, *44*, 4030-4034.

[17] Lin, L.; Argon, A. S. Structure and plastic deformation of polyethylene. *J. Material Sci*. **1994**, *29*, 294-323; and refs. therein.

[18] Seguela, R. Critical review of the molecular topology of semicrystalline polymers: The origin and assessment of intercrystalline tie molecules and chain entanglements. *J. Polym. Sci.: Part B: Polym. Phys.* **2005**, *43*, 1729-1748.

[19] Men, Y., Rieger, J.; Strobl, G. Role of the entangled amorphous network in tensile deformation of semicrystalline polymers. *Phys. Rev. Letters* **2003**, *91*, 095502-1 – 095502-4.

[20] Iwata, K. Role of entanglements in crystalline polymers 1. Basic theory. *Polymer* **2002**, *43*, 6609-6626.

[21] Seguela, R. On the natural draw ratio of semi-crystalline polymers: Review of the mechanical, physical and molecular aspects. *Macromol. Mater. Engineering* **2007**, *292*, 235-244.

[22] Deblieck, R.; Van Beek, L.; Remerie, K.; Ward, I. M. Failure mechanisms in polyolefines: The role of crazing, shear yielding and the entanglement network. *Polymer* **2011**, *52*, 2979-2990.

[23] Strobl, G. *The Physics of Polymers. Concepts for Understanding Their Structures and Behavior*; Springer: New York, 1997.

[24] De Gennes, P. G. Reptation of a polymer chain in the presence of fixed obstacles. *J. Chem. Phys.* **1971**, *55*, 572-579.

[25] Doi, M.; Edwards, S. *The Theory of Polymer Dynamics*; Oxford University Press: New York, 1988.

[26] Cao, J.; Qin, J.; Milner, S. T. Finding entanglement points in simulated polymer melts. *Macromolecules* **2015**, *48*, 99-110.

[27] Lotz, B.; Miyoshi, T.; Cheng, S. Z. D. 50th Anniversary perspective: Polymer crystals and crystallization: Personal journeys in a challenging research field. *Macromolecules* **2017**, *50*, 5995−6025.

[28] Luo, C.; Kröger, M.; Sommer, J.-U. Entanglements and crystallization of concentrated polymer solutions: Molecular dynamics simulations. *Macromolecules* **2016**, *49*, 9017-9025.

[29] Wang, S.; Yuan, S.; Wang, K.; Chen, W.; Yamada, K.; Barkley, D.; Koga, T.; Hong, Y.-l.; Miyoshi, T. Intramolecular and intermolecular packing in polymer crystallization. *Macromolecules* **2019**, *52*, 4739−4748.

[30] Romano, D.; Andablo-Reyes, E.; Ronca, S.; Rastogi, S. Aluminoxane co-catalysts for the activation of a bis phenoxyimine titanium (IV) catalyst in the synthesis of disentangled ultra-high molecular weight polyethylene. *Polymer* **2015,** *74*, 76-85.

[31] Archer, L. A. Polymer disentanglement in steady-shear flow. *Rheologica Acta* **2001**, *40*, 74-85.

[32] Bärenwald, R.; Champouret, Y.; Saalwächter, K.; Schäler, K. Determination of orientation of the crystalline and amorphous phases in polyethylene by X-ray diffraction. *J. Phys. Chem. B* **2012**, *116*, 13089-13097.

[33] Yao, Y.- F.; Graf, R.; Spiess, H. W.; Lippits, D. R.; Rastogi, S. Morphological differences in semicrystalline polymers: Implications for local dynamics and chain diffusion. *Phys. Rev. E* **2007**, *76*, 060801(R).

[34] Yao, Y.; Chen, Q. From helical jump to chain diffusion: Solid-state NMR study of chain diffusion in semi-crystalline polymers. *Annual Rep. NMR Spectroscopy* **2010**, *69*, 199-224; and refs. therein.

[35] *Handbook of Polymer Crystallization*, Piorkowska, E.; Rutledge, G. C., Eds.; John Wiley & Sons, Inc.: Hoboken, New Jersey, 2013.

[36] Hong, Y.-l.; Chen, W.; Yuan, S.; Kang, J., Miyoshi, T. Chain trajectory of semicrystalline polymers as revealed by solid-state NMR spectroscopy. *ACS Macro Lett*. **2016**, *5*, 355−358.

[37] Litvinov V. M.; De P. P., Eds.; *Spectroscopy of Rubbers and Rubbery Materials*; Rapra Technology: Shawbury, 2002.

[38] Litvinov, V. M.; Ries, M. E.; Henke, A.; Matloka, P.; Baughman, T. Chain entanglements in polyethylenes melts. Why it is studied again? *Macromolecules* **2013**, *46*, 541-547.

[39] Saalwächter, K. Proton multiple-quantum NMR for the study of chain dynamics and structural constraints in polymeric soft materials. *Prog. Nuclear Magn. Res Spectroscopy* **2007**, *51*, 1 - 35.

[40] Kurelec, L.; Teeuwen, M.; Schoffeleers, H.; Deblieck, R. A. C. Strain hardening modulus as a measure of environmental stress crack resistance of high density polyethylene. *Polymer* **2005**, *46*, 6369–6379.

[41] Cazenave, J.; Seguela, R.; Sixou, B.; Germain, Y. Short-term mechanical and structural approaches for the evaluation of polyethylene stress crack resistence. *Polymer* **2006**, *47*, 3904-3914.

[42] Litvinov, V. M.; van Duin, M. Real-time ^{1}H NMR relaxation study of EPDM vulcanization. *Kautschuk Gummi Kunststoffe* **2002**, *55*, 460-463.

[43] McBrierty, V. J.; Packer, K. J. *Nuclear Magnetic Resonance in Solid Polymers*; Cambridge University Press: Cambridge, U. K., 1993.

[44] Kenwright, A. M.; Say, B. J., Eds.; *NMR Spectroscopy of Polymers*; Blackie Academic & Professional: London, 1993.

[45] Hedesiu, C.; Kleppinger, R.; Demco, D. E.; Buda, A.; Blümich, B.; Remerie, K.; Litvinov, V. M. The effect of temperature and annealing on the phase composition, molecular mobility and the thickness of domains in high-density polyethylene. *Polymer* **2007**, *48*, 763-777.

[46] Litvinov, V. Molecular mobility and phase composition in polyolefines: From fundamental to applied research, in *NMR Spectroscopy of Polymers: Innovative Strategies for Complex*

Macromolecules; Cheng, H. N.; Asakura, T.; English, A. D., Eds.; ACS Symposium Series; 2011; Vol. 1077, Chapter 11, pp 179–190.

[47] Agarwal, V.; van Erp, T. B.; Balzano, L.; Gahleitner, M.; Parkinson, M.; Govaert, L. E.; Litvinov, V.; Kentgens, A. P. M. The chemical structure of the amorphous phase of propylene-ethylene random copolymers in relation to their stress-strain properties. *Polymer* **2014**, *55*, 896-905.

[48] Abragam, A. *The Principles of Nuclear Magnetism*; Oxford University Press: Oxford, 1961.

[49] Keith, J.; Fritzsching, K. J.; Mao, K.; Schmidt-Rohr, K. Avoidance of density anomalies as a structural principle for semicrystalline polymers: The importance of chain ends and chain tilt. *Macromolecules* **2017**, *50*, 1521−1540.

[50] Litvinov, V. M.; Mathot, V. B. F. Partitioning of main and side-chain units between different phases: A solid-state ^{13}C NMR inversion-recovery cross-polarization study on a homogeneous, metallocene-based, ethylene-1-octene copolymer. *Solid State Nuclear Magn. Res.* **2002**, *22*, 218-234.

[51] Sajkiewicz, P.; Hashimotob, T.; Saijob, K.; Gradys, A. 'Intermediate phase' in poly(ethylene) as elucidated by the WAXS. Analysis of crystallization kinetics. *Polymer* **2005**, *46*, 513–521.

[52] Jones, J. A.; Hodgkinson, P.; Barker, A. L.; Hore, P. J. Optimal sampling strategies for the measurement of spin-spin relaxation time. *J. Magn. Res., Series B* **1996**, *113*, 25-34.

[53] Jones, J. A. Optimal sampling strategies for the measurement of relaxation times in proteins. *J. Magn. Res.* **1997**, *126,* 283-286.

[54] Weiss, G. H.; Ferretti, J. A. Optimal design of relaxation time experiments. *Progr. NMR Spectroscopy* **1988**, *20*, 317-335.

[55] Litvinov, V. NMR on Elastomers, In *Encyclopedia of Polymeric Nanomaterials*; Kobayashi, S.; Müllen, K.; Eds.; Springer-Verlag: Berlin Heidelberg, 2014.

[56] Litvinov, V. M.; Barendswaard, W.; van Duin, M. The density of chemical crosslinks and chain entanglements in unfilled EPDM vulcanizates as studied with low resolution, solid state ^{1}H NMR. *Rubber Chem. Technol.* **1998**, *71*, 105-118.

[57] Litvinov, V. M. Characterization of chemical and physical networks in rubbery materials using proton NMR magnetization relaxation. In *Spectroscopy of Rubbers and Rubbery Materials*; Litvinov V. M.; De, P. P., Eds.; Rapra Technology Ltd: Shawbury, 2002, p. 353-400.

[58] Gotlib, Y. Y.; Lifshits, M. I.; Shevelev, V. A.; Lishanskii, I. A.; Balanina, I. V. The influence of the chemical crosslinking network on the spin-spin relaxation of crosslinked and swelling polymer systems. *Polym. Sci. USSR* **1976,** *18*, 2630-2636.

[59] Ferry J. D. *Viscoelastic Properties of Polymers*; 3rd ed.; John Wiley & Sons, Ltd.: New York, 1980.

[60] Fry, C. G.; Lind, A. C. Determination of cross-link density in thermoset polymers by use of solid-state ^{1}H NMR techniques. *Macromolecules* **1988**, *21*, 1292-1297.

[61] Aharoni, S. M. On entanglements of flexible and rodlike polymers. *Macromolecules* **1983**, *16*, 1722-1728; ($C_\infty = 7.0$).

[62] Wu, S. Predicting chain conformation and entanglement of polymers from chemical structure. *Polym. Engineering Sci*. **1992**, *32*, 823-830; ($C_\infty = 5.7$).

[63] Wool, R. P. Polymer entanglements. *Macromolecules* **1993**, *26*, 1564-1569; ($C_\infty = 6.7$).

[64] Fetters, L. J.; Lohse, D. J.; Richter, D.; Witten, T. A.; Zirkel, A. Connection between polymer molecular weight, density, chain dimensions, and melt viscoelastic properties. *Macromolecules* **1994**, *27*, 4639-4647; ($C_\infty = 7.3$).

[65] Heymans, N. A novel look at models for polymer entanglements. *Macromolecules* **2000**, *33*, 4226-4234; ($C_\infty = 7.38$).

[66] Litvinov, V. M. Strain-induced phenomena in amorphous and semicrystalline elastomers. Solid state ^{1}H NMR T_2 relaxation under uniaxial compression. *Macromolecules* **2001**, *34*, 8468-8474.

[67] Litvinov, V. M. EPDM/PP thermoplastic vulcanizates as studied by proton NMR relaxation: Phase composition, molecular mobility, network structure in the rubbery phase and network heterogeneity. *Macromolecules* **2006**, *39*, 8727-8741.

[68] Litvinov, V. M.; Dias, A. A. Analysis of network structure of UV-cured acrylates by ^{1}H NMR relaxation, ^{13}C NMR spectroscopy, and dynamic mechanical experiments. *Macromolecules* **2001**, *34*, 4051-4060.

[69] Ries, M. E.; Brereton, M. G.; Ward, I. M.; Cail, J. I.; Stepto, R. F. T. Rescaling approach to molecular orientation for NMR and optical properties of polymer networks. *Macromolecules* **2002**, *35*, 5665-5669.

[70] Schmidt-Rohr, K.; Spiess, H. W. Chain diffusion between crystalline and amorphous regions in polyethylene detected by 2D exchange carbon-13 NMR. *Macromolecules* **1991**, *24*, 5288-5293.

[71] Glowinkowski, S.; Makrocka-Rydzyk, M.; Wanke, S.; Jurga, S. Molecular dynamics in polyethylene and ethylene-1-butene copolymer investigated by NMR methods. *Eur. Polym. J.* **2002**, *38*, 961-969.

[72] Bärenwald, R.; Goerlitz, S.; Godehardt, R.; Osichow, A.; Tong, Q.; Krumova, M.; Mecking, S.; Saalwächter, K. Local flips and chain motion in polyethylene crystallites: A comparison of melt-crystallized samples, reactor powders, and nanocrystals. *Macromolecules* **2014**, *47*, 5163−5173.

[73] Cole, E. A.; Holmes, D. R. Crystal lattice parameters and the thermal expansion of linear paraffin hydrocarbons, including polyethylenes. *J. Polym. Sci*. **1960**, *46*, 245-256.

[74] Swan, P. R. Polyethylene unit cell variations with temperature. *J. Polym. Sci*. **1962**, *56*, 403-407; ibid, Polyethylene unit cell variations with branching. **1962**, *56*, 409-416.

[75] Toda, A.; Tomita, C.; Hikosaka, M.; Saruyama, Y. Melting of polymer crystals observed by temperature modulated d.s.c. and its kinetic modeling. *Polymer* **1998**, *39*, 5093-5104.

[76] Crist, B.; Howard, P. R. Crystallization and melting of model ethylene-butene copolymers. *Macromolecules* **1999**, *32*, 3057-3067.

[77] Wignall, G. D.; Alamo, R. G.; Londono, J. D.; Mandelkern, L.; Kim, M. H.; Lin, L. S.; Brown, G. M. Morphology of blends of linear and short-chain branched polyethylenes in the solid state by small-angle neutron and X-ray scattering, differential scanning calorimetry, and transmission electron microscopy. *Macromolecules* **2000**, *33*, 551-561.

[78] Marand, H.; Huang. Z. Isothermal lamellar thickening in linear polyethylene: Correlation between the evolution of the degree of crystallinity and the melting temperature. *Macromolecules* **2004**, *37*, 6492-6497.

[79] Furushima, Y.; Nakada, M.; Murakami, M.; Yamane, T.; Toda, A.; Schick, C. Method for calculation of the lamellar thickness distribution of not-reorganized linear polyethylene using fast scanning calorimetry in heating. *Macromolecules* **20015,** *48*, 8831-8837.

[80] Sommer, J.-U.; Luo, C. Molecular dynamics simulations of semicrystalline polymers: Crystallization, melting, and reorganization. *J. Polym. Sci.: Part B: Polym. Phys*. **2010**, *48*, 2222–2232.

[81] Melnikov, A.P.; Rosenthal, M.; Ivanov, D.A. Thermal Analysis of Semicrystalline Polymers: Exploring the General Validity of the Technique *ACS MacroLetters* **2018**, *7*, 1426–1431.

[82] Melnikov, A. P.; Rosenthal, M.; Rodygin, A. I.; Doblas, D.; Anokhin, D. V.; Burghammer, M.; Ivanov, D. A. Re-exploring the double-melting behavior of semirigid-chain polymers with an *in-situ* combination of synchrotron nano-focus X-ray scattering and nanocalorimetry. *Eur. Polym. J*. **2016**, *81*, 598-606.

[83] Lotz, B. Analysis of the structure and morphology of crystalline polymers by electron microscopy imaging and diffraction: a personal journey. *Microscopy*, **2014**, *63*, 95–109.

[84] Litvinov, V. M.; Xu, Jianjun; Melian, C.; Demco, D. E.; Möller, M.; Simmelink, J. Morphology, chain dynamics and domain sizes in gel-spun ultra-high molecular weight polyethylene fibers at final stages of drawing by SAXS, WAXS and ^{1}H solid-state NMR. *Macromolecules* **2011**, *44*, 9254-9266.

[85] Fatkullin, N.; Fischer, E.; Mattea, C.; Beginn, U.; Kimmich, R. Polymer dynamics under nanoscopic constraints: the “corset effect” as revealed by NMR relaxometry and diffusometry. *ChemPhysChem* **2004**, *5*, 884-894.

[86] Wischnewski, A.; Monkenbusch, M.; Willner, L.; Richter, D.; Likhtman, A. E.; McLeish, T. C. B.; Farago, B. Molecular observation of contour-length fluctuations limiting topological confinement in polymer melts. *Phys. Rev. Letters* **2002**, *88*, 058301-1 – 058301-4.

[87] Moorthi, K.; Kamio, K.; Ramos, J.; Theodorou, D. N. Monte Carlo simulation of short chain branched polyolefins: Structure and properties. *Macromolecules* **2012**, *45*, 8453−8466; and refs. therein.

[88] Tanabe, Y.; Strobl, G. R.; Fischer, E. W. Surface melting in melt-crystallized linear polyethylene. *Polymer* **1986**, *27*, 1147-1153.

[89] Ivanov, D.A.; Bar, G.; Dosière, M.; Koch, M.H.J. A novel view on crystallization and melting of semirigid chain polymers: The case of poly(trimethylene terephthalate). *Macromolecules* 2008, *41,* 9224-9231.

[90] Flory, P. J.; Yoon, D. Y. Molecular morphology in semicrystalline polymers. *Nature* **1978**, *272*, 226-229.

[91] Kurz, R.; Schulz, M.; Scheliga, A.; Men, Y.; Seidlitz, A.; Thurn-Albrecht, T.; Saalwächter, K. Interplay between crystallization and entanglements in the amorphous phase of the crystal-fixed polymer poly(ε-caprolactone). *Macromolecules* **2018**, *51*, 5831−5841.

[92] Teng, C.; Gao, Y.; Wang, X.; Jiang, W.; Zhang, C.; Wang, R.; Zhou, D.; Xue, G. Reentanglement kinetics of freeze-dried polymers above the glass transition temperature. *Macromolecules* **2012**, *45*, 6648-6651.

[93] Rosenthal, M.; Bar, G.; Burghammer, M.; Ivanov, D.A. On the nature of chirality imparted to achiral polymers by the crystallization process. *Angewandte Chemie: Int. Ed.* **2011**, *123,* 9043-9047.

[94] Luo, C.; Sommer, J.-U. Disentanglement of linear polymer chains toward unentangled crystals. *ACS Macro Lett*. **2013**, *2*, 31−34.

[95] Roy, D.; Roland, C. M. Reentanglement kinetics in polyisobutylene. *Macromolecules* **2013**, *46*, 9403-9408.

[96] Barham, P. J.; Sadler, D. M. A neutron scattering study of the melting behavior of polyethylene single crystals. *Polymer* **1991**, *32*, 393-395.

[97] Ramos, J.; Vega, J. F.; Theodorou, D. N.; Martines-Salazar, J. Entanglement relaxation time in polyethylene: Simulation versus experimental data. *Macromolecules* **2008**, *41*, 2959-2962.

[98] Hall, K. W.; Sirk, T. W.; Klein, M. L.; Shinoda, W. A coarse-grain model for entangled polyethylene melts and polyethylene crystallization. *J. Chem. Phys*. **2019**, *150*, 244901; and refs. therein.

[99] Raju, V. R.; Smith, G. G.; Marin, G.; Knox, J. R.; Graessley, W. W. Properties of amorphous and crystallizable hydrocarbon polymers. I. Melt rheology of fractions of linear polyethylene. *J. Polym. Sci.: Polym. Phys. Ed.* **1979**, *17*, 1183-1195.

[100] Aguilar, M.; Vega, J. F.; Sanz, E.; Martínez-Salazar, J. New aspects on the rheological behaviour of metallocene catalysed polyethylenes. *Polymer* **2001**, *42*, 9713−9721; and refs. 2, 4, 5, 8, 30, 46, 36 and 37 therein.

[101] Szántó, L.; Vogt, R.; Meier, J.; Auhl, D.; Van Ruymbeke, E.; Friedrich, C. Entanglement relaxation time of polyethylene melts from high-frequency rheometry in the mega-hertz range *J. Rheol*. **2017**, *61*, 1023-1033.

[102] Likhtman, A. E.; Ponmurugan, M. Microscopic definition of polymer entanglements. *Macromolecules* **2014**, *47*, 1470-1481.

[103] Likhtman, A. E. The tube axis and entanglements in polymer melts. *Soft Matter* **2014**, *10*, 1895-1904.

[104] Ibar, J.-P. The great myths of polymer melt rheology, Part I: Comparison of experiment and current theory. *J. Macromol. Sci.: Part B: Phys*. **2009**, *48*, 1143−1189.

[105] Lang, M.; Sommer, J.-U. Analysis of entanglement length and segmental order parameter in polymer networks. *Phys. Rev. Letters* **2010**, *104*, 177801-1 - 177801-4.

[106] Doi, M. Explanation for 3.4-power law for viscosity of polymeric liquids on the basis of the tube model. *J. Polym. Sci.: Polym. Phys. Ed*. **1983**, *21*, 667-684.

[107] Saalwächter, K. Comment on "Chain entanglements in polyethylene melts. Why is it studied again?" *Macromolecules* **2013**, *46*, 5090−5093.

[108] Litvinov, V. M.; Ries, M. E.; Henke, A.; Matloka, P.; Baughman, T. Reply to "Comment on 'Chain Entanglements in Polyethylene Melts. Why Is It Studied Again?'" *Macromolecules* **2013**, *46*, 5094-5096.

[109] Lee, J. H.; Fetters, L. J.; Archer, L. A.; Halasa, A. F. Tube dynamics in binary polymer blends. *Macromolecules* **2005,** *38,* 3917-3932.

[110] van Ruymbeke, E.; Shchetnikava, V.; Matsumiya, Y.; Watanabe, H. Dynamic dilution effect in binary blends of linear polymers with well-separated molecular weights. *Macromolecules* **2014**, *47*, 7653−7665.

[111] Wagner, M. H. The effect of dynamic tube dilation on chain stretch in nonlinear polymer melt rheology. *J. Non-Newtonian Fluid Mech.* **2011**, *166*, 915–924.

[112] Brown, H. R. A Molecular interpretation of the toughness of glassy polymers. *Macromolecules* **1991**, *24*, 2752-2756.

[113] Kramer, E. J.; Berger, L. L. Fundamental process of craze growth and fracture. *Adv. Polym. Sci.* **1990**, *91-92*, 1-68.

[114] Kramer, E. J. *Adv. Polym. Sci*. Microscopic and molecular fundamentals of crazing. **1983**, *52-53*, 1–56.

[115] Plummer, C. J. G. Microdeformation and fracture in bulk polyolefins. *Adv. Polym. Sci*. **2004**, *169*, 75-120.

[116] Van den fonteyne, W. H. W. The effect of molecular architecture on the deformation behaviour of drawn bimodal polyethylene. *PhD Thesis*, University of Leeds, 2016.

[117] Litvinov, V. M.; Kurelec, L. Remarkably high mobility of some chain segments in the amorphous phase of strained HDPE. **2014**, *Polymer*, *55*, 620-625.

[118] Hedesiu, C.; Demco, D. E.; Remerie, K.; Blümich, B.; Litvinov, V. M. Study of uniaxially stretched isotactic poly(propylene) by ^{1}H solid-state and IR spectroscopy. *Macromolecular Chemistry Physics* **2008**, *2009*, 734-745.

[119] Men, Y.; Rieger, J.; Enderle, H.; Lilge, D. The mobility of the amorphous phase in polyethylene as a determining factor for slow crack growth. *Eur. Phys. J.: E, Soft Matter* **2004**, *15*, 421-425.

[120] VanderHart, D. L.; Pérez, E. A carbon-13 NMR method for determining the partitioning of end groups and side branches between the crystalline and noncrystalline regions in polyethylene. *Macromolecules* **1986**, *19*, 1902-1909.

[121] Pérez, E.; VanderHart, D. L.; Crist Jr., B.; Howard, P. R. Morphological partitioning of ethyl branches in polyethylene by carbon-13 NMR. *Macromolecules* **1987**, *20*, 78-87.

[122] Rasburn, J.; Klein, P. G.; Ward, I. M. The influence of short-chain branching on the creep behavior of oriented polyethylene, and its effect of the efficiency of crosslinking by electron irradiation. *J. Polym. Sci.: Part B: Polym. Phys*. **1994**, *32*, 1329-1338.

[123] Steenbrink, A. C.; Litvinov, V. M.; Gaymans, R. J. Toughening of SAN with acrylic core-shell rubber particles: Particle size effect or cross-link density? *Polymer* **1998**, *39*, 4817-4825.